Building and Environment 190 (2021) 107538

Contents lists available at ScienceDirect

Building and Environment

journal homepage: http://www.elsevier.com/locate/buildenv

Review on ventilation rates in the ventilated air-spaces behind common wall assemblies with external cladding

Mohammad Rahiminejad *, Dolaana Khovalyg

Thermal Engineering for the Built Environment Laboratory (TEBEL), Ecole Polytechnique Fédérale de Lausanne (EPFL), Lausanne, Switzerland

ARTICLE INFO

Keywords:
Ventilated facade
External cladding
Stack effect
Wind effect
Air change rate

ABSTRACT

For many decades, ventilated cavities in wall assemblies of buildings have been essential for creating moisture resilient constructions by allowing airflow within the air gap to promote drying. In addition to that, the airflow in the cavity can enhance the thermal performance of the building envelope, depending on the air change rate and outdoor conditions. Therefore, the effective factors on the air change rate in the ventilated cavity behind common wall assemblies with external cladding are specified in the present study. As a first step, the analysis of the stack effect and wind effect as mechanisms that drive the airflow in the ventilated air-space available in the literature is reviewed. Moreover, the hydraulic network of pressure losses along the wall cavity is analyzed, and various correlations for the loss factors are described. Despite separate studies analyzing the effect of the ventilated cavity on moisture dissipation through water-permeable materials, a comprehensive overview of the airflow rates behind the ventilated wall assemblies is still lacking. Therefore, as the second step in this paper, existing methods of predicting air-change rates behind the ventilated cladding systems are classified and compared with the measured data. The amount of air change rate in the ventilated air gaps behind brick, cement & stucco, ceramic, wood, and other types of external facades are studied through a comprehensive review of relevant publications. Based on the observations, the maximum air change rate in the air-spaces behind open joint claddings such as the ceramic wall is nearly two times compared to the closed joint claddings such as the brick wall.

1. Introduction

A ventilated wall assembly consists of three main layers: a wall core adjacent to the interior side of the building, a cladding that is exposed to the outdoor, and a ventilated air gap that separates the wall core from the cladding. Ventilated air-space has an inlets opening and the outlets opening, the air can enter either from the bottom or the top opening. An illustration of a typical ventilated facade is shown in Fig. 1.

A wall assembly that incorporates an air-space behind its cladding can significantly reduce energy use and boost the thermal efficiency of the building [1]. Particularly, in the cooling seasons, higher thermal resistance efficiencies could be achieved by replacing the enclosed cavity with the ventilated air gap [1–3]. This practice can also be used as a rain control strategy to provide drainage of incidental moisture by eliminating capillary flows between the cladding and sheathing [4].

It is becoming more common in North America to construct walls with cladding separated from the framed wall by an air-cavity [5–7]. Different types of external cladding materials have been used in the building structures. In particular, an overview of external cladding materials used in new single-family homes is performed using market analysis with special attention to the U.S.A. The historical trend of material used in 2010 and 2017 is presented in Fig. 2. It should be noted that similar market data was not available for commercial buildings. Overall, based on the market review performed, vinyl siding is the most common type of external cladding material used in the U.S.A for residential buildings. In comparison to the other types of exterior wall materials, the use of brick cladding had little change, while the use of fiber cement and stucco positively trended upward in recent years [8].

In addition to the type of material, external claddings are categorized according to their types of joints that can be closed or open. As illustrated in Fig. 3, the closed joint facades are those in which external cladding is continuous, while the open joint facades are claddings with some air gaps in the external wall. More specifically, the term “Open Joint Ventilated Façades” (OJVF), refers to a building system in which an external layer of slabs or tiles (metallic, ceramic, stone, or composite) is hanged using a metallic-frame structure to the exterior face of the

* Corresponding author.
E-mail address: mohammad.rahiminejad@epfl.ch (M. Rahiminejad).

https://doi.org/10.1016/j.buildenv.2020.107538
Received 6 October 2020; Received in revised form 1 December 2020; Accepted 16 December 2020
Available online 29 December 2020

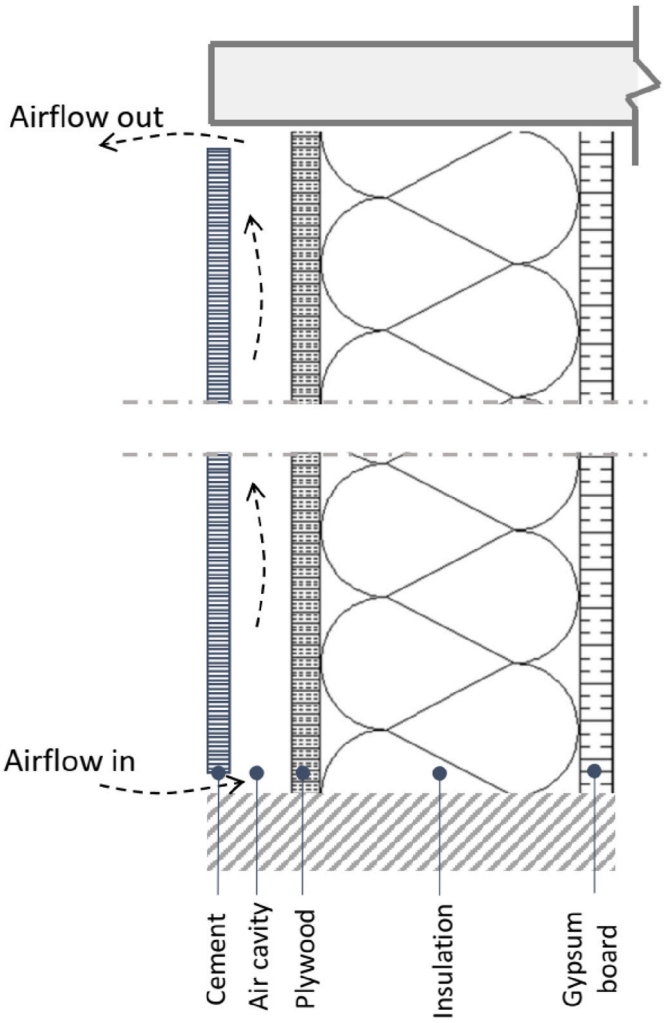

Fig. 1. Basic scheme of the ventilated cavity with external cement cladding (illustration for the upward flow).

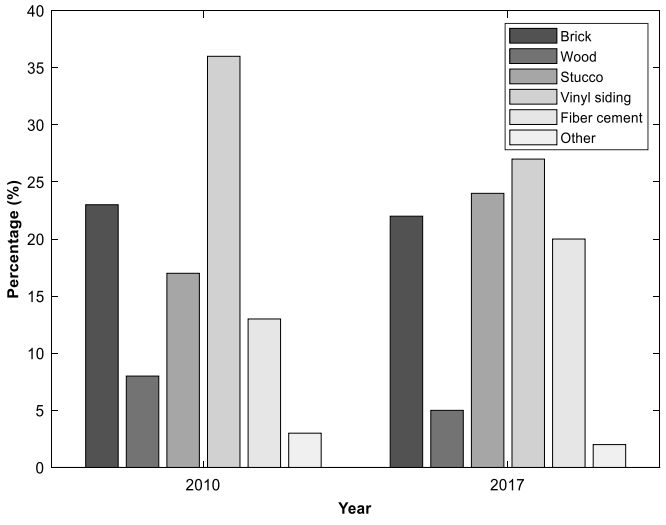

Fig. 2. Percentage variation of different types of external cladding in residential buildings in the U.S.A [8].

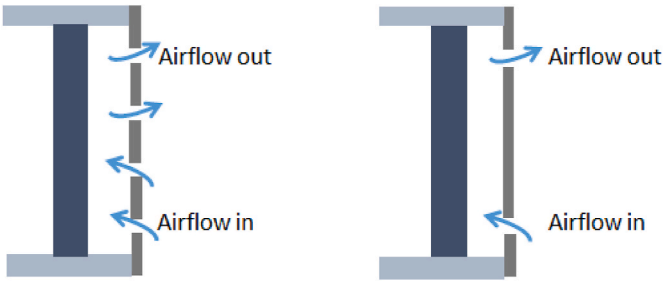

Fig. 3. Types of joints in the external claddings: open joint (left) and closed joint (right).

brick wall, creating an air cavity between wall and slabs. The arrangement of slabs is such that it forms open gaps between them, allowing the surrounding air to enter and leave the cavity all along the façade.

The variation of thermo-hydrodynamic properties in the ventilated air gap is potentially influenced by the amount of airflow in the cavity. The air change rate in the air-space not only determines the rate of moisture removal from the water-absorbent materials but also can promote the thermal performance of the total assembly and provide durable wall systems. Furthermore, updated and accurate data on the thermal performance of air-cavities behind cladding systems need to come at a time when the market is interested in novel solutions to comply with increasingly stringent standards for energy performance, such as ASHRAE Standard 90.1 [9]. Despite this importance, a comprehensive review to address the range of airflow rate in the ventilated cavity behind different types of external claddings is still lacking. Several studies in the literature have tried to theoretically or experimentally quantify the airflow rate in the ventilated air-spaces behind various types of external claddings [5,10–19]. However, a study that classifies the amount of air change rate in the ventilated cavity behind different types of external façades under various environmental and thermo-physical conditions is not available in the literature.

The present study aims to (i) identify the factors that impact air change rates in air-cavities behind cladding systems, (ii) evaluate any existing methods of predicting realistic air change rates, and (iii) explore the literature to quantify the ventilation rates behind common types of claddings. To carry out the review, appropriate research publications by searching different keywords including “cavity ventilation”, “air cavity behind cladding”, “cavity wall”, “ventilated facade”, “ventilated cavity”, etc. were collected. The collected database includes research papers, academic Master degree or Ph.D. thesis, books, independent or market reports, and websites. It is necessary to emphasize that the review is limited to papers focusing on vertical air gaps behind common claddings. Thus, the review excludes non-vertical claddings such as roof claddings that may have some angle of inclination. Additionally, the maximum size of the air gap was limited to 0.49 ft (0.15 m), and wider air gaps such as part of Double Skin Facades were not included in this study. Modern claddings that include Solar PV panels and Phase Change Materials (PCMs) were also excluded from this study since the main focus of the study is to investigate common conventional claddings such as lap siding (e.g., wood, cement, vinyl), anchored brick, veneer, and stucco. Thus, the present study reports research papers that mention ventilation rates in terms of air velocity, air change rate per hour, or air mass flow rate behind air gaps of Opaque Ventilated Facades (OVF). In the following section, the review of the factors that affect the air change rate in the ventilated air-spaces is provided. Thereafter, the air change rate in cavities behind different types of common external claddings reported in the literature is reviewed in section 3. Finally, the discussion on the results and conclusions are provided in section 4 and section 5.

2. Review of factors affecting air change rates in ventilated air cavities behind common claddings

There are several factors that impact air-exchange rates in ventilated air cavities behind external claddings. The air change rate inside the ventilated cavity is a balance between driving forces (wind effect and stack effect) and the pressure resistance along the air passage. The aim of this section is to show the complexity of the airflow in ventilated air cavities and its dependence on the multitude of parameters. The effective parameters on the airflow rate in the ventilated cavity behind opaque ventilated cladding systems are reviewed in this section.

Generally, air change rate primarily depends on average air velocity (or air flow rate) in the cavity [15]:

$$ACH = \frac{u_m}{H} \cdot 3600 \tag{1}$$

$$ACH = \frac{Q}{Volume} \cdot 3600 \tag{2}$$

Under idealized analysis assuming a distinct airflow pathway with a defined inlet and outlet conditions and known boundary conditions, average air velocity u_m can be determined either straightforward by accounting for the wind and thermal fraction of airflow as expressed by equation (3), or, most commonly, by analyzing the balance between the driving mechanism dragging flow through the channel and the total pressure resistance along the flow path as expressed with equations (4) and (5).

$$\dot{V}_{total} = \dot{V}_{wind} + \dot{V}_{thermal} \tag{3}$$

$$\Delta P_{total} = \Delta P_{wind} + \Delta P_{buoyancy} \tag{4}$$

$$\Delta P_{total} = \Delta P_{cavity} + \Delta P_{local\ losses} \tag{5}$$

The driving pressure drop at the steady-state condition is balanced by the overall pressure resistance in the wall cavity that will be discussed later (section 2.3). Analysis of equations (4) and (5) allows determining the average air velocity in the cavity according to the second approach. The following sections will discuss in detail analytical descriptions of defining airflow speed in the wall cavity and, consequently, will analyze parameters that affect the airflow rate.

2.1. Total air volume flow rate in the cavity

As indicated in equation (3), the total air volume flow rate in the cavity $\dot{V}_{total}$ is a sum of the fraction $\dot{V}_{wind}$ due to the wind effect and fraction $\dot{V}_{thermal}$ due to the thermal effect [20].

The wind-induced fraction can be expressed as:

$$\dot{V}_{wind} = C_v\, A_{in}\, V_{wind} \tag{6}$$

Regarding the wind speed V_{wind}, an approximate expression to correct for height differences and terrain characteristics is given in by Hagentoft [21]. Considering the annual median wind speed V_m (at the closest official weather station and height of 32.8 ft (10 m), one can use the below formula to calculate the wind speed at a specific height of the test model:

$$V_H = V_m \cdot k \cdot H^a \tag{7}$$

For the constants, k and a, the following values can be applied: urban area 0.35 and 0.25, and within the city 0.21 and 0.33 [16,21].

In a more complicated procedure, wind speed could be determined using Atmospheric Boundary Layer (ABL) formulas. The ABL is the layer where the flow is directly influenced by the surface of the Earth, and where the flow is retarded by surface friction [22]. By concentrating on the surface layer, meaning the lowest 10–20% of the ABL, the mean wind speed as a function of height in the ABL can be estimated using the logarithmic wind profile [23,24]:

$$V_H = \begin{cases} \frac{u_*}{\kappa} \ln\left(\frac{10}{H_0}\right) & H \le H_d + 10 \\ \frac{u_*}{\kappa} \ln\left(\frac{H - H_d}{H_0}\right) & H \ge H_d + 10 \end{cases} \tag{8}$$

The displacement height (H_d) is the height at which the wind speed would go to zero if the logarithmic wind profile was maintained from the outer flow down into the surface boundary layer. In other words, it is the distance above the ground at which a non-vegetated surface should be placed to provide a logarithmic wind field equal to the observed one [25]. Values of H_0 range from about 0.008 in. (0.02 cm) for the open sea and 0.82 ft (0.25 m) for rural land with few large obstacles to greater than 6.6 ft (2 m) in city centers [26].

The aerodynamic roughness length H_0 is not a real obstacle height, but a measure of the size of eddies at the surface. Bottoma [22] and Gudum [26] provided a roughness classification that is described for the visual determination of roughness length.

Swami and Chandra [27] suggested a correlation between the velocities in two different heights when the reference velocity is measured in one class of terrain and one height, and calculated according to another class of terrain in another height. They classified different types of landscape into 5 categories [26]. For instance, for rural areas with low buildings, the b value should be taken as 0.2 and the a value as 0.85 [26,27].

$$V_{ref} = V_{vH} = \left(\frac{33}{h}\right)^{b_r} \cdot \left(\frac{H}{33}\right)^{b_b} \cdot \frac{a_b}{a_r} \cdot V_{wind,\ rh} \tag{9}$$

A typical range of coefficients C_v values in equation (6) is 0.25–0.35 for diagonal wind and 0.5–0.6 for perpendicular wind [28]. Manuel et al. [29] also reported the same values for C_v. However, they mentioned that by using the above equation for the effect of wind velocity, a notorious discrepancy was observed when air speed inside the channel was examined. This led to an improved model by changing the induced wind velocity inside the channel into a function of the wind direction:

$$C_v\, A_{in} = 0.04 + 0.12\, Cos\,(\pi + W_{dir}) \tag{10}$$

Thermal velocity can be obtained from the energy conservation principle, as proposed by Griffith [30]:

$$\frac{1}{2}\, k \cdot V_{thermal}^2 = \frac{(\rho_{ext} - \rho_{ave,cav})}{\rho_{ave,cav}} \cdot g \cdot L \tag{11}$$

The constant k can be expressed as:

$$\frac{1}{\sqrt{k}} = C_D\, A_{in} \tag{12}$$

The stack induced velocity, for air considered as a perfect gas, can be expressed as:

$$V_{thermal} = C_D\, A_{in} \sqrt{\frac{2gL\left|T_{ave,cav} - T_{ext}\right|}{T_{ext}}} \tag{13}$$

The constant C_D depends on the shape of the inlet and outlet ports of the channel [29]. ASHRAE Handbook of Fundamentals [31] provides a typical range of C_D values varying from 0 to 1.5 and a fixed value (0.65) for unidirectional airflow rate [28].

2.2. Pressure balance in the cavity

2.2.1. Wind effect

Wind effect can be expressed either using wind-induced pressure coefficient C_p (most often) or coefficient C_p of entrance and exit vents; the following subsections will review these two approaches.

1) Wind-induced pressure (wind pressure coefficient C_p)

The magnitude of the external wind pressure depends on the wind speed and the shape of the obstacle [20], and, typically, it is reported as non-dimensional pressure coefficients from field measurements, wind tunnel testing, and modeling. The expression for the wind pressure relative to outdoor pressure is the following [20]:

$$P_{wind} = C_p\left(\frac{1}{2}\rho V_{wind}^2\right) \tag{14}$$

Wind pressure coefficient C_p is influenced by a wide range of parameters, including wind speed, wind direction, building geometry, building height, facade detailing (in case that the façade produces a rough surface that alters wind flow effects), position on the façade, and the degree of exposure/sheltering (local topography which makes variations in the turbulence created by exposure sheltering).

The wind pressure coefficient can be determined for a certain angle of wind as $C_p(\theta)$ using data from wind tunnel experiments. Harmonic interpolation between tabulated angles can be applied for an arbitrary wind angle, an example formula for wind pressure coefficient $C_p(\theta)$ at angle θ (angle of the wind relative to the normal) is shown below [20,31]:

$$C_p(\theta) = \frac{1}{2}\left\{\left[C_p(0^o)+C_p(180^o)\right].\left(Cos^2(\theta)\right)^{\frac{1}{4}} + \left[C_p(0^o)-C_p(180^o)\right].\left(Cos^2(\theta)\right)^{\frac{3}{4}} + \left[C_p(90^o)+C_p(270^o)\right].\left(Sin^2(\theta)\right)^2 + \left[C_p(90^o)-C_p(270^o)\right].(Sin\,(\theta))\right\} \tag{15}$$

2) Wind-induced pressure (wind pressure coefficient C_p of vents)

Wind pressure-induced can also be written in terms of the wind speed at roof height $V_{wind,\,H}$ and wind pressure coefficients of top ($C_p^{top\ vent}$) and bottom ($C_p^{bottom\ vent}$) vents as follows [13]:

$$\Delta P_{wind} = \left(\frac{1}{2}\rho V_{wind,H}^2\right)\left(C_p^{top\ vent} - C_p^{bottom\ vent}\right) \tag{16}$$

Similar to the previous approach, the wind pressure coefficient C_p depends on wind velocity at the level of the roof and wind direction. For example, if the building is assumed to be in an urban residential setting surrounded by other buildings and trees of similar height, pressure coefficients from Bowen [32], as summarized by Liddament [33], can be chosen to represent the top and bottom vents at 10% and 80% of the building height [13]. In the case of the un-partitioned brick veneer cavity, it is necessary to calculate the pressure coefficient to represent the pressure in the cavity C_p^{cavity}. The cavity wind pressure coefficient is defined in the usual way so that the wind pressure difference across a vent ΔP_{wind} can be expressed as follows:

$$\Delta P_{wind} = \left(\frac{1}{2}\rho V_{wind,H}^2\right)\left(C_p^{cavity} - C_p^{vent}\right) \tag{17}$$

The value of C_p^{cavity} can be determined iteratively by considering mass balance in the airflows into and out of the cavity. For an idealized building, having equal ventilation areas on each of the north, south, east and west faces and an unrestrictive cavity, the value of C_p^{cavity} varies from −0.16 to −0.18 depending on wind direction. If all wind directions are equally likely, the average value of $(\sqrt{C_p^{cavity} - C_p^{vent}})$ can be calculated as the equivalent value of $(C_p^{cavity} - C_p^{vent}) = 0.13$. If the cavity is partitioned vertically by battens, then the cavity no longer acts as a conduit connecting all of the vents. In this case, the cavity ventilation process can be modeled as a series of unconnected vertical conduits, each connected to a top and bottom vent. If the top and bottom vents are the same sizes, C_p^{cavity} is simply the average of the $C_p^{top\ vent}$ and $C_p^{bottom\ vent}$. Averaged over all wind directions and wall orientations, the C_p difference for a partitioned cavity is as follows: $(C_p^{cavity} - C_p^{vent}) = 0.10$ [13].

Lateral pressure differences rather than vertical may be more significant, particularly in regions of flow separation and then reconnection to the building surface. Flutter (spatial variation in localized pressures as turbulent wind flow reconnects with a building surface) can also significantly affect porous cladding air change rates. It seems that either method to estimate pressure difference and wind-induced airflow or change in an air cavity behind cladding is over-simplified or assumes idealistic conditions.

2.2.2. Stack effect

The buoyancy-driven pressure differences between the top and bottom vents of a cavity can be expressed in terms of the absolute temperatures $T_{ave,cav}$, T_{ext} and the height H in SI units as follows [13]:

$$\Delta P_{stack} = \left[\left(\frac{352}{T_{ave,cav}} - \frac{345}{T_{ave,cav}^2}\right) - \left(\frac{352}{T_{ext}} - \frac{345}{T_{ext}^2}\right)\right] gH \tag{18}$$

The squared terms can be ignored at room temperatures, so the stack pressure difference driving ventilation through a cavity can be simplified to the following expression [13,17]:

$$\Delta P_{stack} = 3465\left[\left(\frac{1}{T_{ave,cav}}\right) - \left(\frac{1}{T_{ext}}\right)\right] H \tag{19}$$

The buoyancy-driven pressure drop requires knowledge of the average air temperature $T_{ave,cav}$ inside the cavity, which can be determined by solving the heat transfer problem across the building envelope.

It should be noted that air in the cavity and outdoors (exterior) is a combination of dry air and water vapor, and the induced pressure differential is due to thermal, and moisture buoyancy, but the effect of moisture buoyancy is negligible for some types of claddings [5,17,19,34–38].

2.3. Pressure losses

The driving pressure through the wall cavity is balanced by pressure losses at a steady state. Pressure losses along the wall cavity can be modeled as a continuous hydraulic network by using a well-established Darcy-Weisbach relationship [5,11–13,15,18,26,38–44]. The steady-state method divides the total pressure drop into a sequence of air resistances caused by the local friction effect [18]. Depending on the flow structure and geometry of the air gap, the pressure drop in a ventilated wall cavity can be comprised of several contributions, as illustrated in Fig. 4 [43]. Assuming an upward direction of the airflow, the pressure losses in ventilated and screened wall systems are the following: local pressure loss through the bottom opening, e.g., inlet vent (Δp_{bot}), local pressure loss due to the change of the airstream direction at the bottom ($\Delta p_{ch,\,bot}$), pressure loss due to friction in the ventilated chamber (Δp_{wall}), local pressure loss caused by the change of the air stream directly at the exit ($\Delta p_{ch,\,top}$), and local pressure loss through the top opening, e.g., exit vent (Δp_{top}).

Pressure losses in the air gap, having a general form expressed by equation (5), can be specified as follows:

$$\Delta P_{driv} = f\cdot\frac{H\cdot\rho_a.u_m^2}{2\cdot d_H} + \sum_{i=1}^{k}\xi_i.\frac{\rho_a.u_{m,i}^2}{2} \tag{20}$$

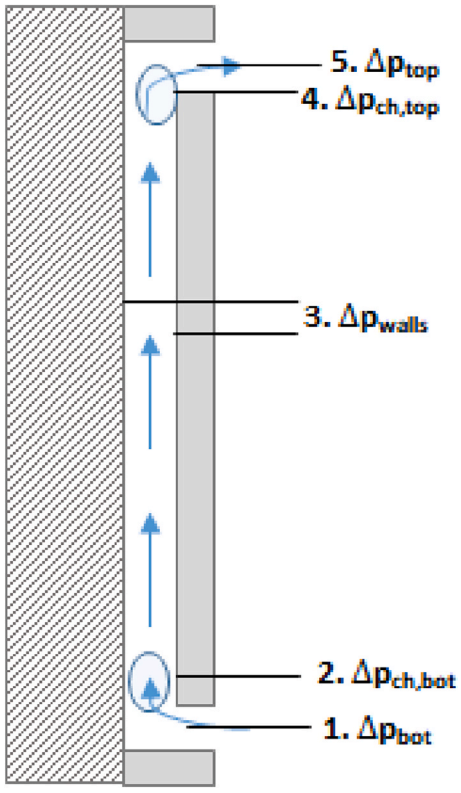

Fig. 4. Pressure losses in ventilated screened wall systems (adopted from Davidovic et al. [43]).

The first part of the above equation (20) is the pressure loss due to moving air through the cavity channel. Assuming that airflow in the cavity is laminar and applying the Darcy-Weisbach equation, the following relationship can be derived between the pressure drop ΔP and the flow rate Q in a cavity [13]:

$$\Delta P_{driv} = \frac{Q \cdot H}{4611 \cdot \gamma \cdot d^3 \cdot w} \tag{21}$$

The roughness factor γ can be equal to unity ($\gamma = 1$) for clear cavities and as the fractional reduction in the cross-section of the cavity for channels with obstructions, according to Basset and McNeil [13]. The blockage factor for mortar protrusions in the brick veneer cavity can be taken as $\gamma = 0.8$ [38].

The second part of equation (20) is the sum of all pressure losses due to the local factors such as obstacles (e.g., vented battens, bug screens), sudden changes in the flow area (entrance/exit), and sudden changes in the flow direction (bends) [15]. Equation (20) can be rearranged as follows [15]:

$$\Delta P_{driv} = \left(f \cdot \frac{H}{d_H} \cdot \left(\frac{1}{A_c^2}\right) + \sum_{i=1}^{k} \xi_i \cdot \left(\frac{1}{A_i^2}\right) \right) \cdot \frac{\rho_a \cdot Q^2}{2} = \psi \cdot \frac{\rho_a \cdot Q^2}{2} \tag{22}$$

By rearranging, the airflow rate can be expressed as:

$$Q = \sqrt{\frac{2 \cdot \Delta P_{driv}}{\psi \cdot \rho_a}} \tag{23}$$

The coefficient ψ includes all geometrical (H d_H, A_c, A_i) and flow parameters (γ, ξ_i)that characterize airflow at a given pressure differential.

2.3.1. Friction factor (f)

Friction factors for airflow in parallel-sided duct for different flow regimes (laminar, transitional, turbulent) are given in equation (24) according to Ref. [41]:

$$f = \begin{cases} \dfrac{64}{\left[\frac{2}{3} + \frac{11}{24}\frac{d}{w}\left(2 - \frac{d}{w}\right)\right] \cdot Re}, & Re \le 2300 \\ \dfrac{(3500 - Re) f^{Re=2300} + (Re - 2300) f^{Re=2300}}{1200}, & 2300 < Re < 3500 \\ \left[2 \cdot \log\left(\dfrac{-4.793}{Re} \cdot \log\left(\dfrac{10}{Re} + 0.2\dfrac{\varepsilon}{d_H}\right) + 0.2698\dfrac{\varepsilon}{d_H}\right)\right]^{-2}, & Re \ge 3500 \end{cases} \tag{24}$$

Pinon et al. [5] recommended the following equations for the friction factor:

$$f = \frac{96}{Re} \quad \text{for} \quad \mathrm{Re} < 1000 \tag{25}$$

$$\begin{aligned} &\lambda' = 0.11 \cdot \left(\frac{12 \cdot \varepsilon}{d_H} + \frac{68}{Re}\right)^{0.25} \\ &f = 0.85\lambda' + 0.0028 \quad if\ \mathrm{Re} > 1000, \lambda' < 0.018 \\ &f = \lambda' \quad if\ \mathrm{Re} > 1000, \lambda' \ge 0.018 \end{aligned} \tag{26}$$

2.3.2. Local loss factors (ξ_i)

Local flow disturbances created, for example, by vent openings and bends introduce pressure losses that can be considered by loss factors ξ_i. Generally, the total pressure loss in the air cavity cannot be treated simply as a sum of local pressure losses without considering their complex interaction. However, some researchers argue that interaction can be ignored because air velocities at the inlet are very low [38], and, similarly, pressure losses caused by expansion at the vent outlets can be negligible due to the relatively low momentum of the air stream [43]. For the configuration of a typical brick veneer cladding, this system can be subdivided into some consecutive resistance elements from bottom to top of the cavity: vented plastic profile/bug screens ($\xi_{vp/bs}$), entrance (open head joint) (ξ_{en}), entrance and exit bends (ξ_{be}), losses in the air channel (ξ_c), exit (open head joint) (ξ_{ex}), vented battens in the top of the cavity (ξ_{vb}). Considering equation (22), an explicit expression for local loss factors is following [15,18]:

$$\begin{aligned} \sum_{i=1}^{k} \xi_i \cdot \left(\frac{1}{A_i^2}\right) = {} & \xi_{vp/bs} \cdot \left(\frac{1}{A_{vp/bs}^2}\right) + \xi_{be} \cdot \left(\frac{1}{A_c^2}\right) + \xi_{en} \cdot \left(\frac{1}{A_{en}^2}\right) + \xi_c \cdot \left(\frac{1}{A_c^2}\right) \\ & + \xi_{ex} \cdot \left(\frac{1}{A_{ex}^2}\right) + \xi_{vb} \cdot \left(\frac{1}{A_{vb}^2}\right) \end{aligned} \tag{27}$$

2.3.2.1. Entrance and exit loss factors (ξ_{en}, ξ_{ex}).

Relations to determine entrance and exit loss factors in parallel-sided unobstructed ducts are given by Kronval [41] in case of the turbulent flow:

$$\xi_{en} = (1 + \sigma)^2 + K_c \tag{28}$$

$$\xi_{ex} = K_e - (1 - \sigma)^2 \tag{29}$$

Straube et al. [12] adopted Idelchik's equation [45] to calculate friction loss factors for laminar and transitional flow as follows [46]:

$$\xi_{en} = 6.5Re^{-0.4} + 0.5 \cdot (0.066 \ln(Re) + 0.16) \tag{30}$$

$$\xi_{ex} = 6.5Re^{-0.4} + (0.066 \ln(Re) + 0.16) \tag{31}$$

The above-mentioned equations 28–31 are applicable for unobstructed openings/exits. However, the entrance of air cavities with external claddings are typically screened using perforated profiles/bug screens.

2.3.2.2. Vented profile/bug screen loss factor ($\xi_{vp/bs}$).

Opening for the airflow at the bottom part of the cladding is typically screened by a

vented profile/bug screen that is intended to prevent intrusion of birds, bugs, or rodents and to enhance aesthetics.

To estimate the magnitude of loss factors due to the perforated vented plastic profile, laboratory tests were performed by Ref. [15]. The profile was perforated with parallel rows of holes 0.013 ft × 0.026 ft (4 mm × 8 mm). For this particular geometry, the losses are expressed by equation (32) where $u_{m,vp}$ is the velocity in the vented plastic profile.

$$\xi_{vp/bs} = \begin{cases} 2.9 - 2.3u_{m,vp} & u_{m,vp} \leq 0.5 \\ 1.9 - 0.3u_{m,vp} & 0.5 < u_{m,vp} \leq 1.5 \\ 1.4 & u_{m,vp} > 1.5 \end{cases} \quad (32)$$

Airflow through a range of vents was measured by Straube and Burnett [38], who confirmed the validity of the following power law between the airflow rate Q through an open vent (excluding capillary type vents) and the driving pressure difference ΔP:

$$Q = A.C_d.\left(\frac{2.\Delta P}{\rho}\right)^n \quad (33)$$

The value of C_d that accounts for frictional losses for perpendicular openings in a brick veneer wall was found to be $C_d = 0.63$ [13]. A flow exponent of $n = 0.5$ indicates that the flow is completely turbulent, e.g., flow-through sharp orifices and large openings. An exponent of $n = 1.0$ indicates that the flow is completely laminar, e.g., flow-through small cracks [42].

Slot type vents (such as a continuous slot at the base of a wall panel) are often better described in terms of the following formula involving a friction factor ξ:

$$\Delta P = \xi.\frac{\rho}{2}.\left(\frac{Q}{A}\right)^2 \quad (34)$$

Typical values for loss coefficients are $\xi = 0.5$ for entry into a slot type vent, and $\xi = 0.88$ for air leaving the opening [13].

2.3.2.3. Loss factor due to vented battens (ξ_{vb}). The top opening might be covered by a vented batten (metal flashing) that forces the airflow to bend when leaving or entering the cavity. This flashing may also cause a reduction of the flow area compared with the nominal cavity area. For a brick cavity, Falk and Sandin [15] through laboratory tests of two vented battens shown in Fig. 5 expressed the vented battens loss factor using average air velocity $u_{m,vb}$ as follows:

$$\xi_{vb} = \begin{cases} 2 & Type\ A \\ 2.8 - 1.4u_{m,vb} + 0.47u_{m,vb}^2 & Type\ B \end{cases} \quad (35)$$

2.3.2.4. Losses due to bending (ξ_{be}). Falk and Sandin [15] evaluated the pressure losses due to the bends, and they pointed that it was not possible to distinguish between the pressure drops due to cavity entrance, friction, and the bend itself. As a result, they approximated contributions of the bend losses from measurements of frictional losses at the entrance by subtracting entrance losses:

$$\xi_{be} = \xi_{be,mausured} - \xi_{en} \quad (36)$$

The bend loss factor for a brick cavity through the laboratory tests for three bend geometries shown in Fig. 6 are the following:

$$\xi_{be} = \begin{cases} 1.8 - 0.3u_m & Type\ 1 \\ 6.0 - 0.7u_m & Type\ 2 \\ 16.8 - 4.3u_m & Type\ 3 \end{cases} \quad (37)$$

Hens [47] recommended the following expression for bend losses ξ_{be} for a rectangular elbow or return depending on the cavity depth d_1 and the entry slot depth d_2 [46]:

$$\xi_{be} = 0.885 \cdot \left(\frac{d_1}{d_2}\right)^{-0.86} \quad (38)$$

Experimental results by Piñon et al. [5,11] showed that the vent-elbow-cavity losses are, generally, coupled and closely spaced vents can interact with each other and a simple way to model complex behavior is recommended.

2.3.2.5. Cavity losses (ξ_c). Davidovic et al. [43] reviewed models to determine local pressure losses in ventilated air cavities using available empirical models. According to their review, "crack flow" and "power law" are two common methods that can be easily employed to calculate the pressure losses in the air-space. Although the entire range of the air change rate, different shapes of the cavity, and variation of local disturbances cannot be evaluated using these methods, the rates of air permeability through the wall assemblies can be obtained by applying the latter model. The "power-law" equation can be favorably used for various opening types and flow regimes.

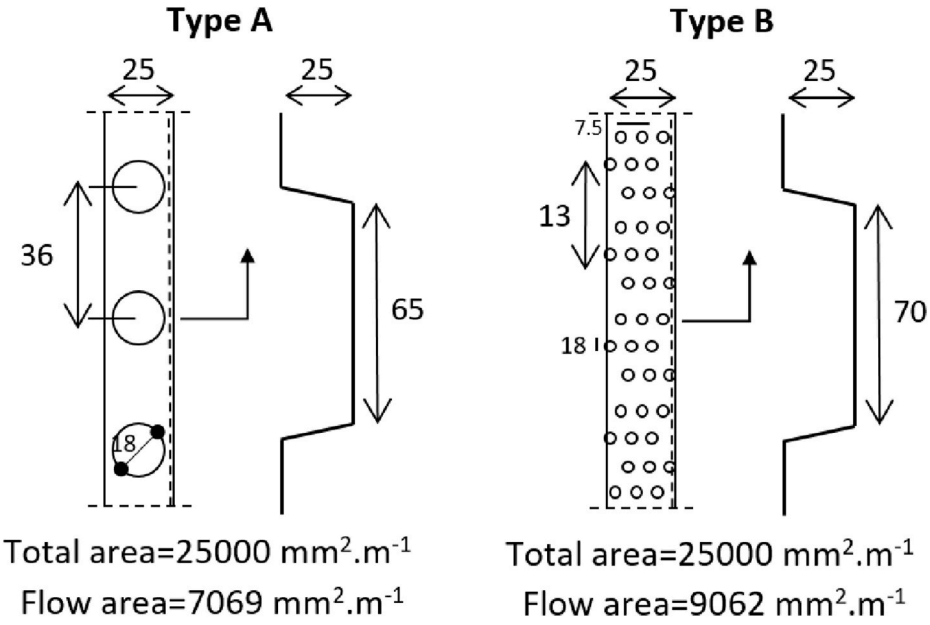

Fig. 5. Different vented battens geometries investigated (adopted from Falk & Sandin [15]).

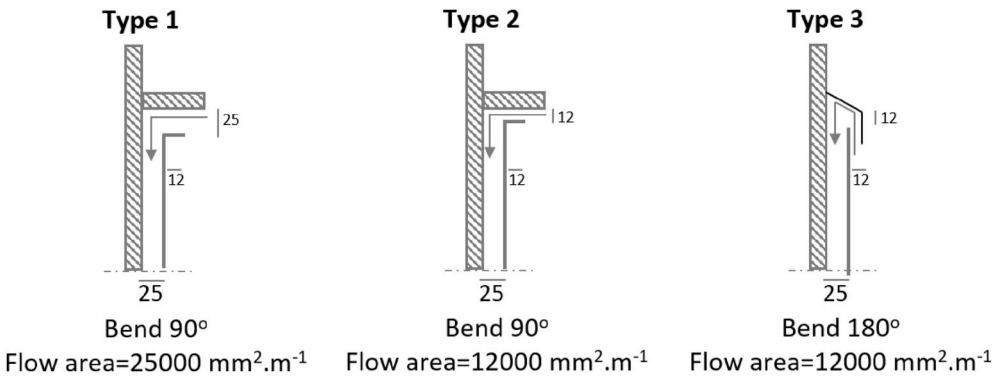

Fig. 6. Different bend geometries investigated (adopted from Falk & Sandin [15]).

2.4. Discussion on the factors affecting the airflow rate in wall cavities

As shown in the previous subsections, the hydrodynamic behavior of the airflow in ventilated air cavities is quite complex and depends on a multitude of parameters. The air change rate inside the ventilated cavity is a balance between the driving forces (wind effect and stack effect) and the pressure resistance along the air passage. As described in section 2.2.1, the wind effect occurs due to the wind-induced pressure difference between the openings of the air cavity, including other unquantified leakage pathways that add uncertainty to idealized predictions. The strength of the wind effect depends on the magnitude of the wind speed, its direction, the orientation of the wall (windward or leeward), and the location of the opening and closing vents. The stack effect explained in section 2.2.2 is created by the density difference of air along the channel that is a function of the heat transfer across the wall assembly, which is a very complex phenomenon and accounts for the thermal network from outdoors to indoors. The main parameter affecting the strength of the buoyancy effect is solar radiation (for walls exposed to solar radiation). The stack effect follows the diurnal temperature changes and reaches its maximum when the solar radiation peaks; therefore, the temperature-induced airspeed reaches its maximum at the same time as well. Besides, the stack effect is greater in summer rather than in winter. Moreover, the stack effect and the wind effect are coupled due to the dependence of the convective heat transfer from the airspeed both outdoors and inside the wall cavity. Static parameters that affect the driving potentials are the properties of building materials (emissivity, thermal conductivity, thickness) and the geometry of the air cavity (depth, height, openings, *etc.*). Generally, changing the opening (inlets and outlets) configuration and its uniformity will have strong effects on the airflow through the air gap. Driving forces are balanced by hydraulic resistance of the air passage shown in section 2.3, which depends on the local pressure loss coefficient, airspeed, and cross-sectional area of the passage.

Considering the review of factors described in the previous subsections, the effect of the studs, junctions, connections, and anchors on the airflow behavior inside the air gap is rarely considered in the literature. Obviously, the corresponding thermal bridges, airflow blockage, and recirculation zones will change the air change rate in the ventilated cavity. It is necessary to mention the effect of air permeability of the external cladding material and wall assembly on an airflow rate inside the cavity. Claddings such as porous brick or masonry walls are permeable to air under the impact of wind or temperature-induced pressure differences, and this can affect heat transfer and airflow in the ventilated air cavity. In addition, it worth mentioning that most of the analyses in the literature have not considered the air change mechanism caused by non-rigid cladding under turbulent wind flow (e.g., flutter that can pump air in and then back out of a given leakage path or port or seam).

3. Ventilation rates behind common ventilated cladding systems

As described in section 2, airspeed and the corresponding airflow rate in ventilated cavities depend on many parameters that are interlinked with each other. In this section, the literature on ventilated facades is categorized based on materials used in the external claddings, and the results on ventilation rates in terms of the velocity magnitude (minimum and maximum values) are reported. The subsections overview the following types of facades: Brick, Cement & stucco, Wood, Ceramic, and other types of claddings (Plexiglas, Metal Panels, Zinc Titanium, Copper, Steel, Clay, Iron, Polyester, and not defined external claddings). For those papers that did not report air velocities but reported ventilation rates (in terms of l/s, m^3/h, etc.) or air change rates per hour (1/h), the values were converted into the velocity magnitudes determined by knowing the geometry of the cavity. If air velocity is reported, ACH was determined using equation (1).

Different methods, including theoretical calculations, numerical analysis, and CFD simulations, can help determine the airflow rate in ventilated air cavities to a certain extent. In the theoretical calculations, either wind effect, stack effect, or pressure losses are considered, and the problem is solved according to the inputs for needed parameters. In the numerical analysis, researchers try to solve the problem using energy balance equations in simple geometries by developing computational codes so that the main variables of the problem can be obtained easily. While employing the numerical model may ease the problem, certain phenomena such as the turbulence effects are hard to be captured. Moreover, some parameters, such as the heat transfer coefficients, are implemented in the numerical analysis using the correlations from experiments that might not precisely match the conditions of the problem. To overcome these drawbacks, Computational Fluid Dynamics (CFD) approach can be used to solve mathematical problems involving fluid flow, heat transfer, mass transfer, etc., even for complicated geometries as long as initial conditions (IC) and boundary conditions (BC) are formulated properly [48,49]. Different approaches in CFD, including the finite volume method, Lattice Boltzmann, RANS, etc., can be employed to solve the chain of Navier-Stokes and energy equations for the entire computational domain. The use of this cost-effective alternative approach provides detailed information on a flow field compared to regular laboratory measurements [48]. A summary of the advantages and disadvantages of different methods is provided in Table 1.

3.1. Brick cladding

The basic purpose of external cladding is protection, and brick is one of the common materials used to protect the building envelope from impacts such as strong winds. The thickness of the brick wall used in the literature reviewed is up to 0.39 ft (0.12 m) with varying thermal properties according to the type of material used. Due to its high thickness, conductivity, and heat storage capacity, brick cladding can

Table 1
Comparison of different methods of predicting ACHs behind ventilated claddings.

Methods	Advantages	Disadvantages
Theoretical (by solving hydraulic network)	o The least-cost & time-consuming method	o Limited accuracy o Rely on extra measurements o No information about distribution (spatial profile) of parameters
Numerical analysis	o Lower cost & time-consuming method than CFD, but higher than theoretical methods o Provides information about the distribution of parameters	o Limited accuracy o Rely on extra measurements (empirical parameters)
CFD simulations	o More reliable than theory & computation methods in case of careful formulation of BC and IC o More accurate compared to theory & numerical approach in case of careful formulation of BC and IC o Provides spatial and temporal variation of parameters	o The most time-consuming method o Largely depends on the knowledge and experience of the user o Rely on extra measurements for validation

significantly affect the thermo-hydrodynamic behavior of the airflow in the cavity. In particular, the temperature gradient in the external cladding caused by the solar flux can impact the stack effect in the cavity and consequently affect the airflow rate in the air-space. Moreover, the wind effect in the air gap is influenced by the type of openings in brick cladding, which can have different shapes (single slot, multiple slots, rectangular, circular, etc.).

Theoretical calculations using the hydraulic network is applied by Lorente [50] to determine the velocity magnitude in a ventilated brick wall considering the certain climatic conditions reported by Lorente and Massias [51]. Results showed that a double ascending air motion caused by the effect of solar radiation. Van Straaten et al. [52] performed calculations of the airflow velocity based on the measured pressure gradient across the cavity. They showed that the wind speed between 4.6 and 19.4 ft/s (1.4 and 5.9 m/s) correlates to horizontal cavity airspeeds of 0.1 and 3.6 ft/s (0.03 and 0.5 m/s) and vertical airspeeds of 0.01 and 0.2 ft/s (0.004 and 0.06 m/s). The work of Finch and Straube [14] showed that by removing the bug-screen inserts from the openings, the ventilation rate could be increased by a factor of ten for similar driving pressures.

In a few studies, numerical analysis is performed to predict the airflow rate in the air-space. For instance, Manuel et al. [29] developed a mathematical model to improve the description of the thermal response of a ventilated façade. The wind direction was introduced to the existing models as a new parameter, which could influence the air velocity inside the channel.

Among different methods, CFD simulations are mostly used in the previous publications to determine the airflow rate in the cavity behind the brick cladding. In the paper by Balocco [53], 3-D transient simulations were performed to investigate the thermal performance of a naturally ventilated brick panel. The results showed the significance of the infiltration passages present in the wall cavities. The thermo-fluid dynamic behavior of three different types of ventilated facades was examined by Patania et al. [54] to study the velocity and temperature profiles under different conditions of incident solar radiation, outdoor temperature, and inlet velocity. The flow of air inside the duct was laminar with a mean velocity of 1.64 ft/s (0.5 m/s). In work by Van Belleghem et al. [55], a ventilated cavity behind a brick wall was analyzed using a coupled Computational Fluid Dynamics–Heat, Air, and Moisture model (CFD-HAM). It was shown that the stack effect and fluctuations in the weather conditions could cause reversed flow in the air-space. Gagliano et al. [56,57] investigated the thermal behavior of an opaque naturally ventilated brick cladding using CFD simulations considering different scenarios for the wind velocity directions. Based on the results, under the calm wind scenario, only the buoyancy effect generated the airflow, and it was directly affected by the incident solar radiation on the facade. In a windward scenario, the outdoor wind speed was the main influential parameter. In a leeward scenario, mixed convection was dominant, and the airflow was influenced by buoyancy and wind forces.

In some research works, experimental measurements are provided by the authors to support the simulation results. Hannan and Derome [58] compared simulations with the measured data to study air movement inside the air cavity of a brick wall. Based on the reported results, during the maximum exposure to solar radiation, air velocity reached its maximum value equal to 0.59–0.82 ft/s (0.18–0.25 m/s). Buratti et al. [59] aimed to obtain good ventilation by possibly having a low number of openings in the cladding. The results showed that decreasing the number of openings can enhance the uniformity of the flow within the air gap. Other studies performed experimental measurements to quantify the actual airflow rate in the cavity under real outdoor conditions [60,61]. Stazi et al. [62] measured the variation of heat flows and ventilation efficiency to investigate how different materials and thermal masses impact the performance of ventilated facades with narrow cavities. Three real-scale prototypes of ventilated facades were tested, including wall assemblies with (i) a lightweight external enclosure, (ii) a massive layer enclosed in the gap, and (iii) an external massive cladding. The results showed that the third configuration could reduce both the incoming and outgoing heat fluxes. Moreover, it was revealed that the position of the thermal mass in the outer layer could increase the air velocity in the cavity.

Fig. 7(a) shows the range of ACH values that are either reported in the publications reviewed or converted from the mean air velocity in the cavity by applying equation (1) and using available data in each study. The height of the investigated cavity in each study is indicated in the labels. Generally, the air change rates that are predicted using the CFD method are higher compared to the other methods. This is mainly due to the higher velocity in the air-space captured by CFD simulations. The heights of the wall structure considered in the experimental measurements are lower than the other methods, which implies the feasibility of testing in the lower heights in actual conditions. The thickness of the ventilated cavity behind brick cladding is considered in the range of 0.06–0.20 ft (0.02–0.06 m) in the majority of the studies. According to the reported publications focusing on the brick as an external cladding material, a wide range of air change rates in air cavities was observed. Most of the ACH values are lower than 400 1/h; while the measured values in most cases are lower than 50 1/h. The available values of maximum air velocity in the cavity through the literature reviewed are plotted in Fig. 8(a). The type of openings that are used in each study is also indicated in the labels. Based on the observations, the majority of the maximum air velocity reported in the literature is lower than 2.3 ft/s (0.7 m/s). The values are in the range of 0.023–7.38 ft/s (0.007–2.25 m/s). Moreover, most of the studies used single slot openings in the ventilated cavity. The presence of single slot openings in the top and bottom of the air-space can cause less pressure resistance against the airflow compared to the multiple slot openings.

3.2. Cement & stucco cladding

Stucco is an exterior plaster, which can be directly applied to masonry or concrete walls and wood-framed walls. In comparison with the brick wall, the thickness of the cement & stucco claddings used in the previous studies is smaller and reaches up to 0.16 ft (0.05 m). The thermal conductivity of this cladding, however, is higher compared to the brick wall. Therefore, the temperature gradient through the external cladding, in this case is lower than the brick cladding.

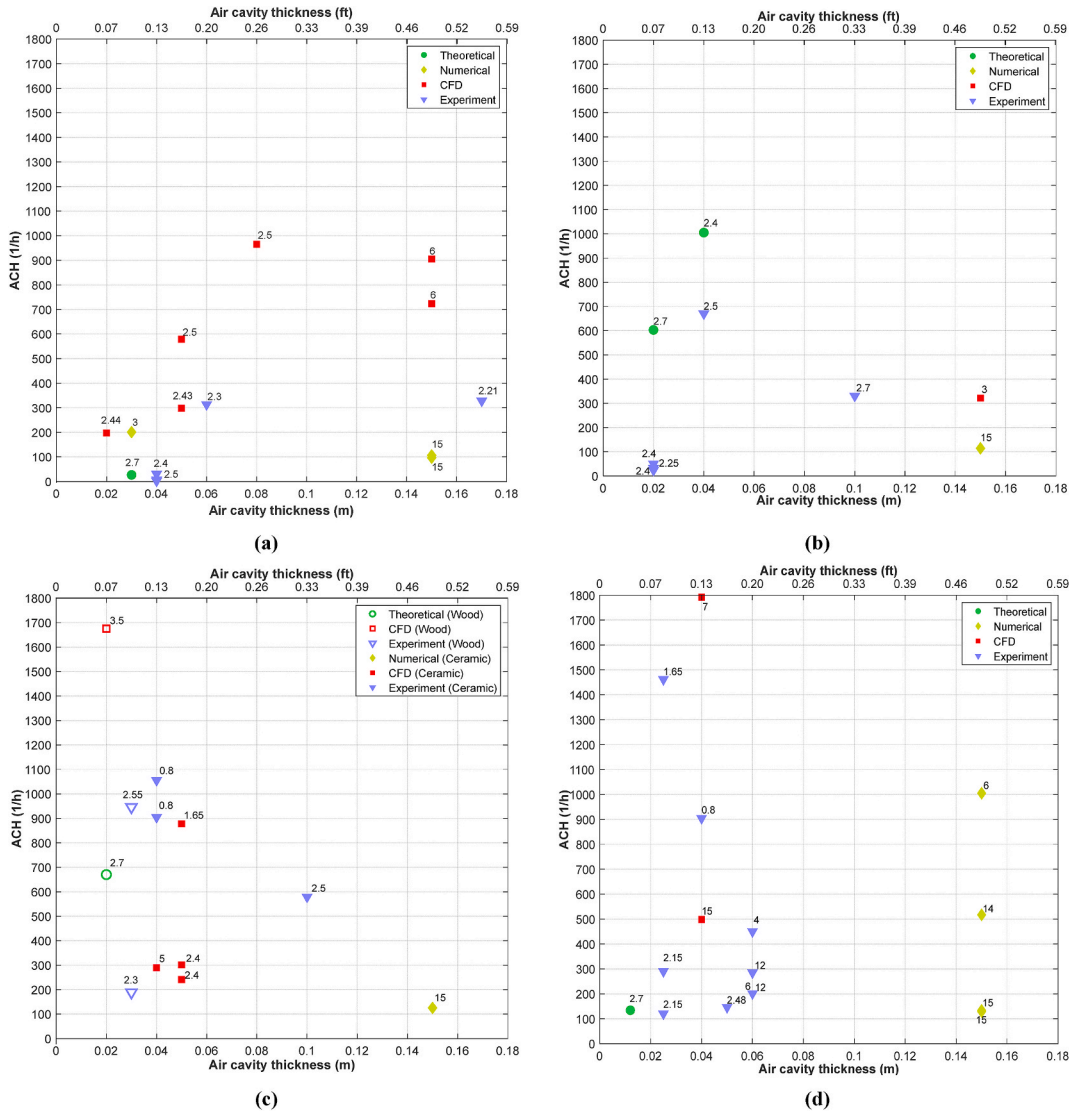

Fig. 7. ACH versus air cavity thickness for (a) brick [3,11,12,14,29,36,44,50–62] (b) cement & stucco [13,18,46,63–66] (c) wood and ceramic [67–78] (d) other types of external claddings [15–17,26,38,79–90] (Labels: height of the cavity (in m)).

A simplified steady-state model was used by Ge and Ye [46] to explore the impact of the ventilated cavity and its opening design on the performance of ventilation drying for a stucco wall. The analysis showed that the cavity ventilation had a minimal influence on the temperature profile within the air cavity.

Prada et al. [63] used CFD simulations and focused on the winter performance of the ventilated walls. It was shown that the airspeed induced by the stack effect is around 0.49–0.66 ft/s (0.15–0.20 m/s) in areas far from the edge regions. Souza et al. [64] studied airflow and heat convection in the air cavity behind a cement cladding in different outdoor conditions. Results showed that the maximum air velocity ranges between 1.15 and 1.18 ft/s (0.35 and 0.36 m/s), while minimum values are in the range of 0.95 and 0.98 ft/s (0.29 and 0.30 m/s).

Bassett and McNeil [13] showed the dependency of the ventilation rates inside the air cavity from the wind pressure and buoyancy pressures. Experimental measurements in drained and ventilated cavities were reported by Bassett and McNeil [65] and showed agreement with the calculated ventilation rates. As part of the later work, Bassett and McNeil [66] used a tracer gas method to measure ventilation rates of different claddings such as brick, fiber-cement, and external insulation finish systems (EIFS). Ventilation rates for open rain-screen walls overlapped with values for drained and ventilated systems, proving the significance of infiltration paths present in these walls. Langmans and Roels [18] investigated two cladding systems including brick veneer and fiber cement sidings. Results indicated that a total pressure difference of 0–2 Pa can cause an air change rate between 100 and 1000 ACH in the sidings, while ventilation rates behind brick veneers were much lower (<10 ACH).

Fig. 7(b) shows the ACH values determined from different research published. Similar to the brick wall, both low and high ACH values can be observed in the literature. The values predicted by the theoretical method are higher compared to the other methods. The thickness of the cavity is mostly considered in the range of 0.06–0.13 ft (0.02–0.04 m). The maximum air velocities in the cavity are plotted in Fig. 8(b). The values start from 0.07 ft/s (0.02 m/s) and reaches up to 3.28 ft/s (1 m/s). Compared to the brick wall, the lower end is higher, while the upper end is lower. The plot also indicates that most of the studies used single slot openings in the ventilated wall assembly.

3.3. *Wood cladding*

The wooden cladding is a common exterior finish for buildings. The thickness of the wooden cladding reported in the literature reviewed reaches up to 0.06 ft (0.02 m). The small air gap is left behind the

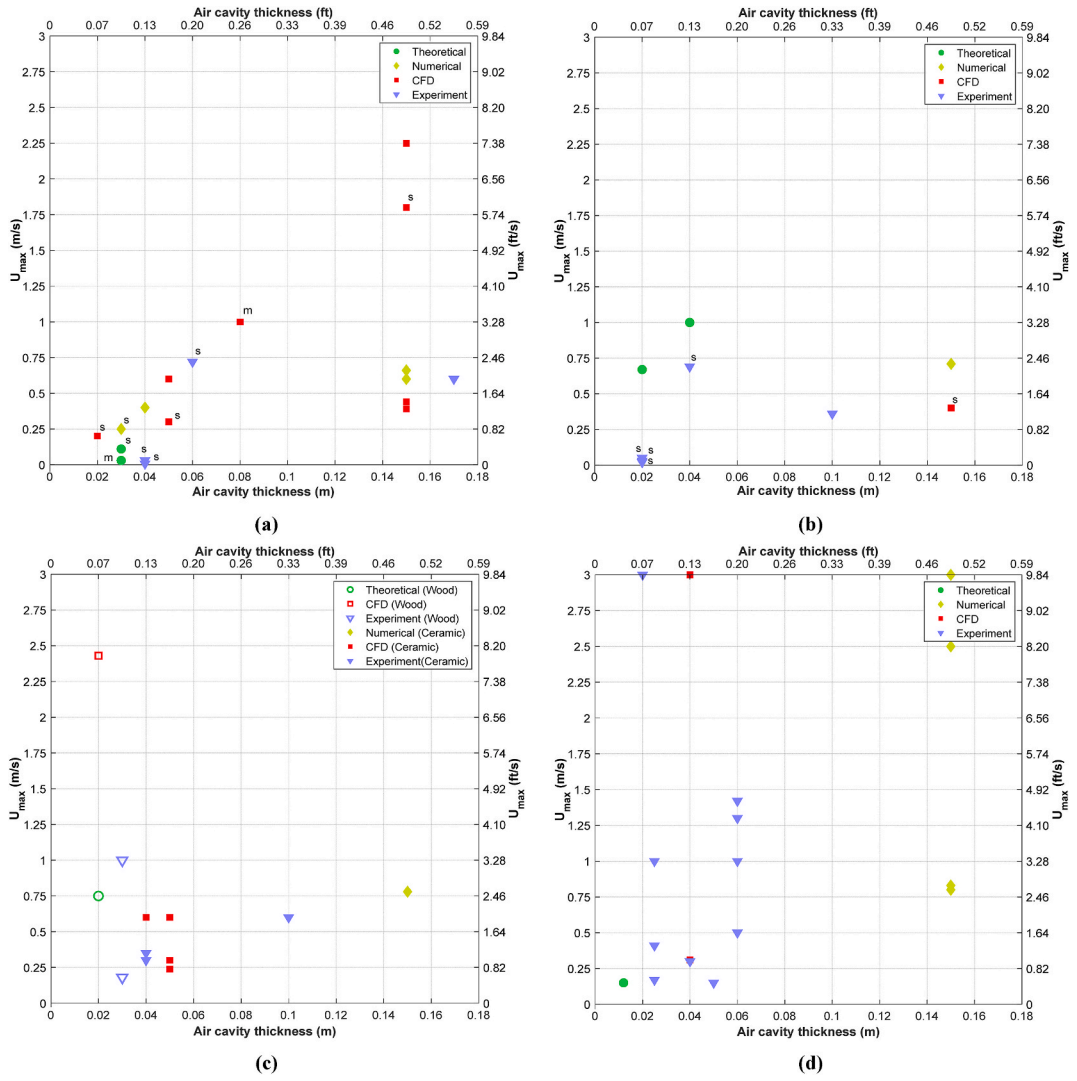

Fig. 8. Maximum air velocity in the cavity versus air cavity thickness for (a) brick [3,11,12,14,29,36,44,50–62] (b) cement & stucco [13,18,46,63–66] (c) wood and ceramic [67–78] (d) other types of external claddings [15–17,26,38,79–90] (Labels: s: single slot; m: multiple slots; blank: not indicated in the publication).

cladding due to the connections between the wall core and the façade. The low thickness and thermal conductivity of this material can cause a negligible temperature gradient in the external cladding. Moreover, the presence of open joints in the wooden cladding can cause perturbations in the hydrodynamic behavior of the airflow inside the cavity. Therefore, the airflow in the cavity is mainly influenced by the wind effect.

Nore et al. [67] performed CFD simulations to study wind-induced airflow in a 0.91 in. (23 mm) ventilated cavity of an isolated low-rise building. The results show that the ratio (ACH/wind speed) was between 120 and 250 for a high reference wind speed of 32.8 ft/s (10 m/s) and the wind direction perpendicular to the facade. The paper presented by Labat et al. [68] focused on the heat transfer phenomena inside the ventilated air gap behind the wooden cladding. The cladding was open-jointed, and it was made up of vertically spaced boards to create air gaps between two adjacent elements. They showed that the temperature of the cladding impacts on the airflow rate, and air velocities could reach up to 0.98 ft/s (0.3 m/s) during the night-time period. Gibson [69] reported the role of the open joint in the ventilated wooden cladding by considering the solar radiation-induced convection. It was observed that air velocities were much higher [0.62 ft/s (0.19 m/s max)] in the open-joint cladding compared to the closed-joint wall [0.23 ft/s (0.07 m/s max)]. Dugue et al. [70] presented a heat transfer model to analyze the heat flow in the air cavity behind opaque wooden claddings. The results showed that the maximum airspeed in the cavity can reach 3.28 ft (1 m/s), and air velocity was always above 0.33 ft (0.1 m/s). Moreover, due to the presence of turbulences at the bottom of the cavity, the measured velocity at the bottom varied more compared to the velocity measured in the middle and on the top, where the airflow was laminar in the latter parts.

According to the results for the ACH values in the ventilated cavity shown in Fig. 7(c), the presence of open joints in the wooden cladding causes higher ventilation rates in the ventilated air-space compared to the brick and cement & stucco claddings. Similar to the brick cladding, the ACH values determined by CFD simulations are higher compared to the other methods. The thickness of the cavity is limited between 0.06 and 0.10 ft (0.02–0.03 m), which implies that the air-space behind wooden cladding is thinner than the closed joint claddings reviewed in the previous sections. Based on the maximum air velocity in the cavity that is plotted in Fig. 8(c), three out of five papers indicate the maximum airspeed to be less than 3.28 ft/s (1 m/s), while the other publication reports greater values [up to 7.9 ft/s (2.4 m/s)]. The lower end of the maximum air velocity behind wooden cladding is higher than the other two types of claddings reviewed in section 3.1 and section 3.2.

3.4. Ceramic cladding

The ventilated cavity behind the ceramic façade is mainly influenced by the open joints between the slabs. The thermal conductivity of this material is higher than the other external claddings reviewed so far in this paper, which alternatively means that the higher surface temperature caused by the solar flux can effectively change the air temperature in the cavity.

Gonzalez et al. [71] introduced the dynamic thermo-fluid behavior of the air in an open joint cladding using CFD techniques. They highlighted that the air movement inside the cavity was three-dimensional and it is necessary to create a 3-D model to properly capture the effect of the joints. Mesado et al. [72] developed a mathematical model using MATLAB® and performed CFD simulations to investigate the behavior of a ventilated façade at a steady-state condition. The results showed that air velocity in the channel could reach up to 0.5 m/s at high solar radiations. Sanjuan et al. [73] developed a 3-D CFD model to study the effect of solar radiation on the airflow in the air gap of an open joint ceramic façade. The results showed that at fixed solar radiation, the mass flow rate in winter is lower compared to summer due to the greater heat flow at lower exterior temperature. Sanjuan et al. [74], in another related paper, described an experimental installation to study the fluid dynamic and thermal characteristics of ventilated façades. The authors mentioned that the total height of the air cavity and the number, size, and distribution of the horizontal joints are fundamental parameters that describe the fluid behavior inside the cavity. Sanchez al [75]. and Sanchez et al. [76] also reported similar conclusions. A complete 3D model and a simplified 2D model of a ventilated cavity were generated by Giancola et al. [77]. Based on the results, the computational cost of 3D was not justified when vertical joints between tiles were sealed and the lateral movement of air was very small. Suarez et al. [78] compared the temperatures and heat transfer fluxes of a typical open joint ventilated façade with a conventional sealed air cavity façade. The air velocity in the open joint cladding was around five times higher than in the sealed facade.

The values of ACH in the cavity behind ceramic cladding are plotted in Fig. 7(c). Since wood and ceramic claddings can theoretically have open joints in their structure, the corresponding ACH values are shown in the same plot. Generally, the values are in a similar range of values for the wooden cladding that was already shown in section 3.3. The air change rate in the air-space behind ceramic cladding starts from 125 1/h which is higher than the lower end of the corresponding value in the brick wall and cement & stucco cladding. It is noticeable that theoretical calculations are not applied for determining the airflow rate in the cavity behind ceramic claddings, which is due to the lack of capability of this method for predicting air flow rate and corresponding pressure drop in the ventilated air-space behind open joint claddings. The range of the thickness of the air cavity investigated in the literature is between 0.13 and 0.20 ft (0.04–0.06 m), which is higher than the values reported for the wooden cladding. Fig. 8(c) shows the maximum values of the air velocity in the cavity behind ceramic walls. Most of the papers provide the maximum air velocity less than 1.97 ft/s (0.6 m/s), while only one study reported greater value [up to 2.56 ft/s (0.78 m/s)]. The upper end of the maximum velocity, in this case, is lower than the case of wooden cladding, while the lower ends are nearly equal.

3.5. Other cladding types

There are other types of materials used as the external cladding in the building structures. This section includes results for the ventilated cavity behind other types of claddings that are not reviewed in the previous sections (i.e. Plexiglas, Metal Panels, Zinc Titanium, Copper, Steel, Clay, Iron, Polyester, etc.). According to the literature reviewed by Silberstein et al. [79], the evaluation of six additional airflow studies on ventilated wall structures confirmed that air velocities in the cavity were generally smaller than 0.98 ft/s (0.3 m/s) for different types of claddings [80]. Assuming continuous openings at the top and bottom as well as a fully developed flow behind the cladding, the maximum amount of ACH over the height of a single-storey building reaches approximately 300 l/h. In the case of a wall that has only some weep holes at the bottom and similar openings at the top, this value is reduced to 20–50 1/h [81]. Mayer and Künzel [34] reported that wind velocity can influence the vertical airspeed in the cavity. It is noted that the impact of wind direction on the airflow rate is more than wind speed. The authors concluded that the cavity airspeed in open slots to 0.79 in. (20 mm) behind smooth panels in 3-storey building, under the condition of 9.8 ft/s (3 m/s) wind speed would be in the range of 0.2–5.25 ft/s (0.06–1.6 m/s).

Balocco [82] simulated a model for a ventilated granite panel by applying a steady-state energy balance to a control volume. The heat transfer throughout the wall was calculated for a channel height of 19.7 and 45.9 ft (6 and 14 m) to compare results with experimental data from the literature [83]. The velocity had a maximum value of 9.84 ft/s (3 m/s). Sanjuan et al. [84] focused on the validation of a 3D model for open joint Iron cladding. The results revealed that ventilation flow in the facade linearly increases by the height of the ventilated cavity. In a study by Peci Lopez et al. [85], a numerical model was created and validated against experimental data. The average airspeed in the cavity behind the steel plate reached a maximum value of 0.49 ft/s (0.15 m/s), while the range of airflow rates measured was from negative values of -177 ft^3/h (-5 m^3/h) (inversed flow) to maximum values over 706 ft^3/h (20 m^3/h). Sagat and Matejka [86] developed a numerical model to evaluate the influence of inlet/outlet insect grilles in naturally ventilated facades on two models with different openings size and geometry. It was observed that the airflow in the model without insect grilles slowly raises from 0.82 ft/s to 1.02 ft/s (0.25 m/s to 0.31 m/s) along with the cavity height.

Straube and Burnett [38] reported research performed by Schwarz [87] to measure the velocity of the airflow in a cavity with open-jointed panel cladding system. The researchers measured velocities of 0.66–1.97 ft/s (0.2–0.6 m/s) under a range of wind speeds of 0–2.6 ft/s (0–8 m/s). It was found that the velocity on the lee side was usually stable at around 0.66 ft/s (0.2 m/s) for the normal range of wind velocities. Jacobsen and Petersen [88] measured air velocity in the cavity behind Plexiglas cladding in the range from 0.66 to 6.6 ft/s (0.2–2 m/s) for wind velocity between 1.6 ft/s (0.5 m/s) and 32.8 ft/s (10 m/s). Using a tracer gas method, the cavity air velocity behind the Plexiglas wall was measured by Gudum [26]. The values were reported as -3.28 ft/s to $+3.28$ ft/s (-1 m/s to $+1$ m/s) for wind velocities in the range of 1.6–32.8 ft/s (0.5–10 m/s) at 15.7 ft/s (4.8 m) above ground level. Stazi et al. [89] presented the results of an experimental study on ventilated clay claddings to assess the thermal performance of the wall assembly under different exposure and various heights of the ventilation channel [19.69 ft and 39.37 ft (6 m and 12 m)]. The measurements showed that doubling the height of the wall increases the airflow rate in the cavity. Falk and Sandin [15] focused on performing field measurements of air velocities and temperatures in the air-spaces behind a rendered & carrier board cladding. For the total measuring time, the average air velocity was found to be 0.64 ft/s (0.195 m/s) in the cavity with vertical battens, while the value reached up to 0.26 ft/s (0.080 m/s) in the air-spaces behind horizontal battens. In another study by Falk and Sandin [16], the airflow model of the ventilated air cavity and basic building physics equations were combined using the same wall geometries as in their earlier study per Falk and Sandin [15]. The main challenge was defined as the calculation of ACH and the evaluation of driving forces due to the thermal buoyancy and wind effect. They simplified the problem by assuming the division of their effect in daylight hours and night-time hours. Calculated ACH values were close to the measured ones indicating that the driving force model was an acceptable approach. In the third study by Falk et al. [17], transient ventilation rates in the air gap were defined and compared with their previous experimental results. The results showed that the simple driving force model could capture the temporal variability inside the air gap, and it was applicable to predict

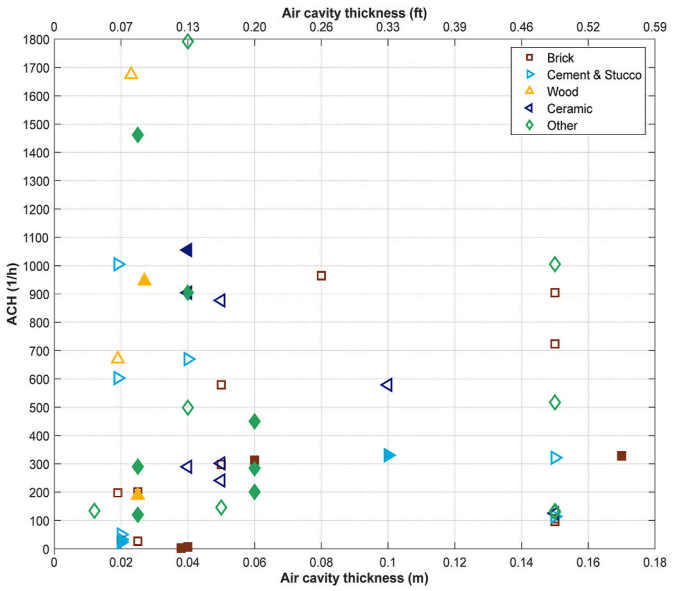

Fig. 9. ACH versus air cavity thickness for different external cladding materials (The markers are filled if the values are measured.).

average ventilation rates. The aim of the experimental study carried out by Stazi et al. [90] was to investigate the thermo-physical performance of ventilated zinc-titanium claddings with different heights. In a day without wind, the average airflow behind the wall with a lower height was about 75 air changes per hour (ACH). For the wall with a higher height, the maximum airflow could reach up to 380 ACH.

Figs. 7(d) and Figure 8(d) respectively provide the ACH and maximum air velocity values behind different cladding types reviewed in this section. According to Fig. 7(d), all methods have been used in the literature for determining the airflow rate in the ventilated air-spaces. A considerable number of studies used experimental measurements to obtain the ACH values. The plots reveal that a wider range of cavity thickness is considered in the related publications. The ACH values are more scattered compared to the corresponding values reviewed in the previous sections. The range of ACH is between 100 and 1800 1/h, while the majority is lower than 600 1/h. Considering the maximum air velocity in the cavity shown in Fig. 8(d), most of the studies reported air velocities less than 4.3 ft/s (1.3 m/s).

4. Discussion

Generally, air velocity (consequently ACH) in the cavity depends on many parameters that can affect the air behavior inside the cavity. The most important parameters that can influence air movement inside the air cavity individually or together are the following: outdoor weather conditions (wind velocity, wind direction, air temperature, solar radiation), material properties of the external cladding and the wall core, dimensions of the air cavity (height, thickness), presence of obstructions and openings, air infiltration through the external cladding, and the presence of the reflective insulation in each side of the air gap. As the global summary of the ACH values in the ventilated air-spaces behind different types of external claddings, Fig. 9 provides an overview found from the literature reviewed in this paper. The figure is prepared considering the accessible data in each research paper for the air gap thickness, mean air velocity (u_m), and height (h) of the air cavity.

The plot in Fig. 9 reveals that building wall assemblies with air cavity thickness in the range 0.07–0.16 ft (0.02–0.05 m) and also around the value of 0.49 ft (0.15 m) were mostly reported. The results show that the ACH values are not consistently distributed for each cladding type. In general, the majority of ACH values are lower than 1000 1/h, and the measured values are below 400 1/h most of the time. It is necessary to account that the ACH rate is sensitive to the height of the cavity that is being described. Therefore, the same air velocity behind different cladding types with different heights can produce different results.

To have a better overview of the results, the minimum and maximum ACH values retrieved from the literature reviewed in this paper is provided in Table 2. The data are categorized based on the method of determination of ACH value in the ventilated cavity behind various cladding types defined in this study. According to the results, the maximum ACH values in the air-spaces determined by CFD simulations are higher than the other methods in the case of using brick, wood, and other types of external claddings. Considering experimental measurements, the maximum air change rate occurs in the air cavity behind the ceramic cladding. The minimum ACH values measured behind wooden and ceramic claddings are much greater than the corresponding values for the brick and cement & stucco claddings. This implies the effect of the open joints in the external claddings on the amount of air change rate in the air-spaces. Considering different types of external claddings reviewed in this paper, one can compare the range of ACH values determined per different methods with the measured data. In the case of the brick wall, the range of air change rate predicted by numerical analysis is within the range of values measured experimentally, while the theoretical calculations and CFD simulations respectively underestimate and overestimate the expected ACH values. In the case of using cement & stucco cladding, both numerical analysis and CFD simulations determined the ACH values within the range of the experimental data, and theoretical calculations predicted higher values. Although theoretical calculations predicted the ACH value in the range of measurements in the case of using wooden cladding, due to having a few available studies, the conclusion on the most suitable method for predicting air change rate behind this type of cladding still needs more research. In the case of ceramic cladding used in the wall assembly, the values determined per CFD simulations have better agreement with the experimental data.

The air ventilation rate behind claddings is a combination of thermal and fluid mechanics, and it is necessary to think of a better way of comparing results from different studies. Perhaps, the better way of analyzing data across different publications would be comparing specific values corresponding to a particular (point-in-time) condition

Table 2
Retrieved data from the literature reviewed for the ACH values behind different ventilated claddings with different methods (The tabulated values are either reported or converted from the mean air velocity in the cavity indicated in the publications).

Method	Theoretical calculation		Numerical analysis		CFD simulation		Experimental measurements	
External cladding	ACH[a] (1/h)							
	min	max	min	max	min	max	min	max
Brick	26.8	26.8	96.5	201	197.7	964.8	2.1	654.8
Cement & stucco	603	1005	114.2	114.2	321.6	321.6	23.6	670
Wood	670	670	–	–	1675	1675	188.8	945.9
Ceramic	–	–	125.4	125.4	241.2	877.1	578.9	1055.3
Other	134	134	128.6	1005	498.5	1791.8	120	1461.8

[a] The equal values of min and max ACH are taken from the same source.

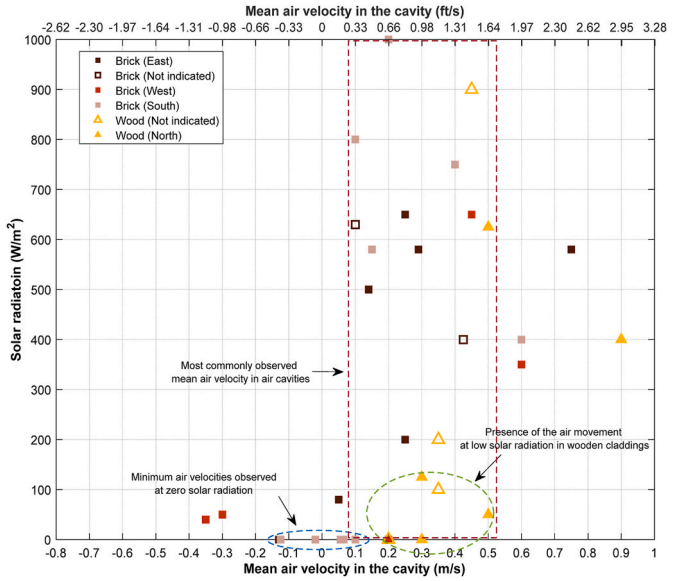

Fig. 10. Mean air velocity in air cavities as a function of solar radiation [3,11,12,14,29,36,44,50–62,67–70].

during a day. Therefore, such a comparison is attempted for selected types of claddings in Fig. 10-Fig. 12.

Fig. 10 shows the effect of solar radiation on the air velocity in the cavity behind brick and wood claddings; the face direction of the investigated wall is also indicated in the figure. Although in some cases, higher air velocities occur at lower values of solar radiation (due to the influence of other parameters), the trend reveals that increasing solar radiation leads to an increase in air velocity inside the cavity. According to the results, the mean air velocity in the cavity is mainly in the range of 0.33–1.64 ft/s (0.1–0.5 m/s), as shown in the dashed box in Fig. 10. As expected, the lowest air cavity velocities are observed when solar radiation is zero (i.e., night condition). The data shown in Fig. 10 reveals that the stack effect caused by solar radiation is more effective in the case of wooden cladding. Although the thermal conductivity of the wooden cladding is lower than the brick cladding, the results show that the mean air velocity in the cavity is higher in the former at the same solar radiation. This can be attributed to the smaller temperature gradient between the outdoor environment and the airflow in the airspace due to a smaller thickness of the wooden cladding. In this case, the back surface of the cladding that is adjacent to the cavity would experience higher temperature caused by the solar radiation, which increases the air temperature in the cavity and consequently enhances the air movement in the air gap. Furthermore, air movements at low solar radiations in wooden claddings imply that the wind effect can be an important factor affecting airflow in the cavity behind wooden claddings. Negative air velocity values in Fig. 10 demonstrate that airflow can be reversed in the absence of solar radiation.

At low solar radiation levels, the stack effect is limited, and the wind effect dominates, which may turn the flow direction downward. Fig. 11 illustrates the effect of wind speed on the air velocity for brick cladding; the way the C_p value was accounted for is noted in the illustration. Also, the wind direction and its angle are indicated assuming 0° for North Wind. Although we expect increased air velocity inside the cavity at greater wind speed, the comparison reveals the opposite tendency – air velocity is very low even at the very strong wind. It is hard to identify the reason behind such behavior without analyzing the multitude of other parameters that affect the airflow rate in the cavity.

Another important parameter is exterior air temperature, which can individually affect air velocity in the cavity. Fig. 12 shows the relation between exterior air temperature and cavity air velocity for different cladding types. The season is indicated in the figure for each data point. As it was expected, the air velocity in the cavity during summertime is higher than in colder seasons in the case of using a brick wall as the external cladding. The trend clearly shows that in winter conditions, air velocity is lower than in Fall and Summer. It means that increasing outdoor temperature causes more air movements in the cavity, which is the direct result of the stack effect. In some cases, the airflow would be downward in the cavity, which reveals the influence of other combined parameters. A similar analysis is provided for Wood, Cement & stucco claddings. Since fewer studies are available in these categories, fewer data points are illustrated. The effect of the outdoor temperature shown in Fig. 12 illustrates a similar behavior as for the brick wall – air velocity is greater in summer rather than in winter.

The main result of the above plots is that the range of air change rates in the ventilated cavity cannot be distinguished for particular cladding systems. According to Fig. 9, there is noticeable uncertainty in predicting an air change rate for any given set of boundary conditions (e.g.,

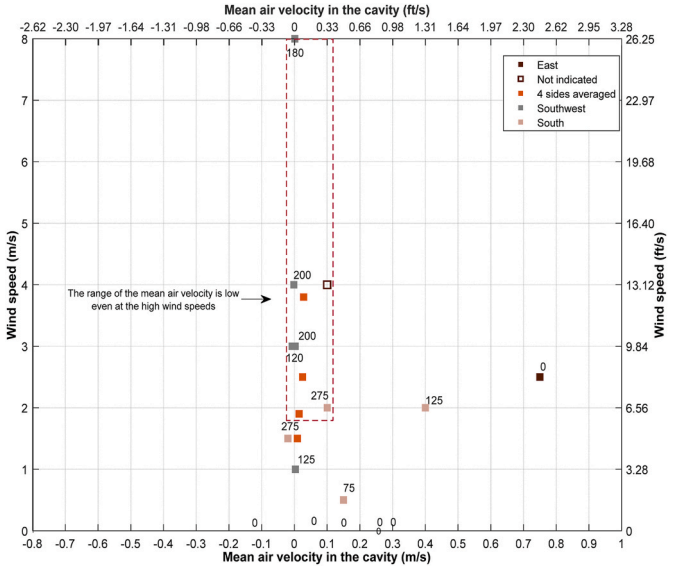

Fig. 11. Wind speed versus mean air velocity in the cavity behind the brick cladding (wind angles are indicated assuming 0° for North wind) [3,11,12,14,29,36,44,50–62].

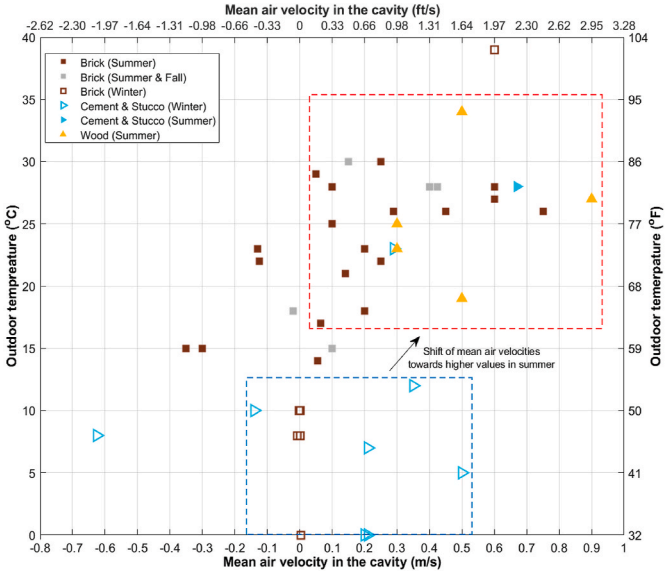

Fig. 12. Outdoor temperature versus mean air velocity in the cavity [3,11–14,18,29,36,44,46,50–70].

wind, solar, etc.), which might relate to energy performance (e.g., thermal resistance) over a typical year.

The primary aim of using the ventilated air-space behind external cladding is to promote drying for creating moisture resilient constructions. The presence of air-space can also impact the thermal performance of the entire wall assembly. However, the thermal performance of the wall structure is a complex phenomenon that can have different dynamics depending on certain conditions. For example, the presence of a ventilated air cavity can be beneficial in terms of energy use of the building envelope in summer, while a closed cavity might be more advantageous compared to the ventilated air-space in winter conditions as shown by Aelenei [1]. Therefore, it is difficult to strictly establish a rule regarding the contribution of the ventilated air-space behind an external cladding in the thermal performance of the building envelope. This issue needs more in-depth analyses of different factors affecting the thermal performance of the wall structure, which can be addressed in future studies.

5. Conclusion

The airflow rate in the air-space behind claddings can play an important role in the thermal performance of the entire assembly. It can change the heat flow in the cavity and consequently can impact the heat flux through the interior surface. The thermo-hydrodynamic behavior of air behind facades is a complex phenomenon influenced by several factors, including the outdoor and indoor conditions, geometrical and thermal properties of the wall layers. Based on the literature reviewed in this study, the stack effect and the wind effect are two major mechanisms driving the airflow in ventilated air-spaces. Accordingly, the air velocity in the air cavity depends on external wind speed and solar radiation, which induces temperature gradient in both horizontal and vertical directions. Different methods, theoretical and numerical, of predicting ACH in ventilated air gaps were also reviewed. The airflow rate in the air gap can be predicted by solving a hydraulic network theoretically and numerically, along with complex simulations using CFD tools. Among the methods for estimating the airflow rate in the cavity, the CFD approach has more capability to detail different aspects of the fluid mechanics and heat transfer mechanisms that occur in the air-space, conditioned that the user has enough knowledge and experience to set the boundary conditions carefully. Due to the complexity of describing the problem of air change rate inside an air gap behind cladding materials, field and laboratory experiments are the essential source of reliable data, especially when it comes to the comparison between different types of walls and conditions.

To define the range of air velocity or the air change rate per hour behind common types of ventilated claddings used in buildings, different external claddings were grouped into 5 types. A comprehensive literature review was performed for wall assemblies with brick, cement & stucco, wood, ceramic, and other types of external claddings. Ventilation rates behind various types of air-spaces with different geometries and under different conditions were collected. The ACH values found in the literature, either directly reported in ACHs or converted to ACHs based on reported air velocity values, were averaged for each type of cladding. According to the reported values in the literature, a wide range of air velocity in air cavities was observed in brick walls. The maximum magnitude of the air velocity behind cement & stucco cladding did not exceed 3.28 ft/s (1 m/s), while it is 7.97 ft/s (2.43 m/s) in the wooden walls. Most of the papers provide the maximum air velocity of lower than 1.97 ft/s (0.6 m/s) for cavities in the ceramic wall assemblies. Regarding other types of external claddings, most of the studies reported air velocities less than 4.92 ft/s (1.5 m/s). The review of measured results revealed that ACH values were below 50 1/h for brick veneer (in most cases), 50 1/h for cement & stucco (in most cases), 950 1/h for wood, and 1055 1/h for ceramic.

Despite multiple studies performed in this field, most of the publications did not consider the effect of air permeability of the external cladding material and the air change mechanism caused by non-rigid cladding under turbulent wind flow (e.g., flutter that can pump air in and then back out of a given leakage path or port or seam). Therefore, further analysis is needed to address these points in future studies. The values provided in this study can help façade designers to have an overview of the magnitude of airflow rate in ventilated air-spaces behind common types of external claddings. This, hopefully, will urge practitioners and engineers to pay attention to the possible effect of the ventilated air cavity on the thermal performance and moisture removal of the entire wall assembly.

Nomenclature

Symbol	Unit IP (SI)	Definition
u	ft/s (m/s)	Mean velocity
H	ft (m)	Height
Q	ft^3/s (m^3/s)	Air flow rate
P	psi (Pa)	Pressure
V	ft/s (m/s)	Speed
C_v	–	Effectiveness of the openings
A	ft^2 (m^2)	Area
u_*	ft/s (m/s)	Friction velocity
κ	–	Von Karman constant (0.4)
H_0	ft (m)	Aerodynamic roughness length
H_d	ft (m)	Displacement height
h	ft (m)	Mast height in the reference terrain
a_r , b_r	–	Terrain constants of the reference terrain
a_b , b_b	–	Terrain constants of the building terrain
W_{dir}	–	Wind direction (azimuthal angle in radian)
ρ	lb/ft^3 (kJ/m^3)	Density
g	ft/s^2 (m/s^2)	Gravity value
L	ft (m)	Height from the midpoint of the lower opening to the Neutral Pressure Level
C_d	–	Discharge coefficient for the opening
T	℉ (°C)	Temperature
C_p	–	Wind pressure coefficient
f	–	Friction factor
ξ	–	Loss factor
γ	–	Cavity blockage factor
w	ft (m)	Width
Re	–	Reynolds number
ε	in (mm)	Roughness of the cavity walls
σ	–	Ratio of the constriction to the frontal area
K_c	–	Contraction loss coefficient
K_e	–	Expansion loss coefficient

Subscripts

a	Air
ave	Average
be	Bending
cav	Cavity
en	entrance
ex	Exit
ext	exterior
H	Hydraulic
in	inlet
m	mean
rh	Reference terrain at height h
vb	vented batten
vH	Reference at height H
vp/bs	vented profile/bog screen
wind	wind

Declaration of competing interest

The authors declare that they have no known competing financial interests or personal relationships that could have appeared to influence

the work reported in this paper.

Acknowledgment

This study was a part of ASHRAE RP-1759 sponsored by the TC 4.4 committee (Building Materials and Building Envelope). It also received financial support from École Polytechnique Fédérale de Lausanne (EPFL). The authors would like to acknowledge the corresponding Project Monitoring Subcommittee members (M. Bianchi, J. Crandell, H. Ge, and P.C.T. Velasco) for their constructive feedback and guidance during the review.

References

[1] L.E. Aelenei, Thermal Performance of a Naturally Ventilated Cavity Wall, 2006.
[2] C. Marinosci, G. Semprini, G.L. Morini, Experimental analysis of the summer thermal performances of a naturally ventilated rainscreen facade building, Energy Build. 72 (2014) 280–287.
[3] M. Ciampi, F. Leccese, G. Tuoni, Ventilated facades energy performance in summer cooling of buildings, Sol. Energy 75 (6) (2003) 491–502.
[4] J. Straube, G. Finch, Report 0906: Ventilated Wall Claddings: Review, Field Performance, and Hygrothermal Modeling. Test, Building Science Corporation, 2009, p. 25.
[5] J. Piñon, D. Davidovic, E. Burnett, J. Srebric, ASHRAE 1091-Report #5. Characterization of ventilation airflow in screened wall systems. The Pennsylvania Housing Research/Resource Center, Pennsylvania State University, 2004.
[6] Cladding Market Analysis by Product (Steel, Aluminum, Composite Panels, Fiber Cement, Terracotta, Ceramic), by Application, Competitive Landscape, and Segment Forecasts, 2018 – 2025. Grand View Research.
[7] R. Fairfax, D.J. Lofgren, D.C. Johnson, T.L. Walley, OSHA compliance issues", J. Occup. Environ. Hyg. 1 (1) (2004) 1–6.
[8] US Bureau of the Census, Construction Report Series, Characteristics of New Housing, US Department of Commerce, Washington, DC, 2017.
[9] A. Standard, ASHRAE Standard 90.1, Energy Standard for Buildings Except Low-Rise Residential Buildings, 2016.
[10] J. Straube, Moisture Control and Enclosure Wall Systems, Univ Waterloo, 1998.
[11] J. Piñon, D. Danko, E. Burnett, J. Srebric, The Airflow Characteristics of Ventilated Cavities in Screen-type Enclosure Wall Systems, RP-1091), 2004.
[12] J. Straube, R. VanStraaten, E. Burnett, C. Schumacher, Review of Literature and Theory, 2004. Report #1. In: ASHRAE 1091-Development of design strategies for rainscreen and sheating membrane performance in wood frame walls. Building Engineering Group. Univ Waterloo.
[13] M.R. Bassett, S. McNeil, The Theory of Ventilation Drying Applied to New Zealand Cavity Walls, vol. 119, 2005.
[14] G. Finch, J. Straube, Ventilated wall claddings: review, field performance and hygrothermal modeling, in: Proceedings of the thermal performance of the exterior envelopes of whole buildings X, Vol 2, 2007. Clearwater, Florida.
[15] J. Falk, K. Sandin, Ventilated rainscreen cladding: measurements of cavity air velocities, estimation of air change rates and evaluation of driving forces, Build. Environ. 59 (2013) 164–176.
[16] J. Falk, K. Sandin, Ventilated rainscreen cladding: a study of the ventilation drying process, Build. Environ. 60 (2013) 173–184.
[17] J. Falk, M. Molnár, O. Larsson, Investigation of a simple approach to predict rainscreen wall ventilation rates for hygrothermal simulation purposes, Build. Environ. 73 (2014) 88–96.
[18] J. Langmans, S. Roels, Experimental analysis of cavity ventilation behind rainscreen cladding systems: a comparison of four measuring techniques, Build. Environ. 87 (2015) 177–192.
[19] M. Vanpachtenbeke, J. Langmans, J. Van den Bulcke, J. Van Acker, S. Roels, On the drying potential of cavity ventilation behind brick veneer cladding: a detailed field study, Build. Environ. 123 (2017) 133–145.
[20] A. Berge, Analysis of Methods to Calculate Air Infiltration for Use in Energy Calculations, 2011, p. 98.
[21] C.E. Hagentoft, Introduction to Building Physics, Studentlitteratur, Lund, 2001.
[22] M. Bottoma, Wind Climate and Urban Geometry, Eindhoven, Technische Universiteit Eindhoven, The Nederlands, 1993, ISBN 90-386-0132-8.
[23] S. Larsen, The Atmospheric Boundary Layer over Land and Sea: Focus on the Offshore Southern Baltic and Southern North Sea Region, 2013, pp. 1–36.
[24] M.L. Orme, M.W. Liddament, A. Wilson, Technical Note 44 - Numerical Data for Air Infiltration and Natural Ventilation Calculations, AIVC, 1998.
[25] P.S. Jackson, J.R.C. Hunt, Turbulent wind flow over a low hill, J. Roy. Met. Soc. 101 (1975) 929–955.
[26] C. Gudum, Moisture Transport and Convection in Building Envelopes, 2003.
[27] M.V. Swami, S. Chandra, Procedures for Calculating Natural Ventilation Airflow Rates in Buildings - Final Report FSEC-CR-163-86, Florida Solar Energy Center, Cape Canaveral, 1987.
[28] V. Corrado, A. Gorrino, S. Paduos, Energy Performance Characterisation of Vented Opaque Envelope through Simplified Methodologies, 2012, pp. 323–332.
[29] V. Manuel, S. Francés, E. José, J. Manuel, E. Bannier, V. Cantavella, G. Silva, Modeling of ventilated facades for energy building simulation software, Energy Build. 65 (2013) 419–428.
[30] B. Griffith, A model for naturally ventilated cavities on the exteriors of opaque building thermal envelopes, Simbuild (2006) 153–159.
[31] ASHRAE. ASHRAE Handbook—Fundamentals. Atlanta, American Society of Heating, Refrigerating and Air-Conditioning Engineers, Inc., 2017.
[32] J.J. Bowen, A Wind Tunnel Investigation Using Simple Building Models to Obtain Mean Surface Wind Pressure Coefficients for Air Infiltration Estimates - NRC Report LTR-LA-209, National Research Council, Canada, 1976.
[33] M. Liddament, Air Filtration Calculation Techniques: an Application Guide, 1999.
[34] E. Mayer, H. Künzel, Untersuchungen über die notwendige Hinterlüftung an Aubenwandbekeidung aus grobformatigen Bauteilen, Franhofer Institut für Bauphysick, Forschungsbericht B Ho 1 (1983) 83.
[35] D. Davidovic, J. Srebric, E.F.P. Burnett, Modeling convective drying of ventilated wall chambers in building enclosures, Int. J. Therm. Sci. 45 (2) (2006) 180–189.
[36] T.K. Stovall, A. Karagiozis, Airflow in the ventilation space behind a rain screen wall, Proc Therm Perform Exter Envel Build IX (2004).
[37] Y. Simpson, Field Evaluation of Ventilation Wetting and Drying of Rainscreen Walls, 2010.
[38] J. Straube, Burnett E. Vents, Ventilation Drying, and Pressure Moderation, 1995.
[39] J. Lecompte, The Influence of Natural Convection on the Thermal Quality of Insulated Cavity Walls Constructions (In Dutch), Laboratorium Bouwfysica, Heverlee, KU Leuven, 1989.
[40] R. Kohonen, Transient analysis of the thermal and moisture physical behaviour of building constructions, Build. Environ. 19 (1) (1984) 1–11.
[41] J. Kronvall, Air Flows in Building Components, Lund Institute of Technology, Lund, 1980.
[42] J.F. Straube, E.F.P. Burnett, "Vents, Ventilation and Masonry Veneer Wall Systems", 1998, pp. 194–207.
[43] D. Davidovic, J. Piñon, E.F.P. Burnett, J. Srebric, Analytical procedures for estimating airflow rates in ventilated, screened wall systems (VSWS), Build. Environ. 47 (1) (2012) 126–137.
[44] R. Van Straaten, Measurement of Ventilation and Drying of Vinyl Siding and Brick Clad Wall Assemblies, 2003.
[45] I.E. Idelchik, Handbook of Hydraulic Resistance, third ed., CRC Press, Boca Raton, Florida, FL, USA, 1994.
[46] H. Ge, Y. Ye, Investigation of ventilation drying of rainscreen walls in the coastal climateof British Columbia, in: Proceedings of Thermal Performance of the Exterior Envelopes of Buildings X, Vol 2, ASHRAE, Florida, 2007.
[47] H. Hens, Bouwfysica 1, Warme - En Massatransport, Leuven, Belgium, 1992.
[48] G.A. Odewole, Airflow Patterns in Ventilated Wall Cavities Gboyega Akindeji Odewole, 2011.
[49] H.K. Versteeg, W. Malalasekera, An Introduction to Computation Fluid Dynamics: the Finite Volume Method, Pearson Education Ltd, England, 1995, ISBN 0-582-21884-5.
[50] S. Lorente, Heat losses through building walls with closed, open and deformable cavities, Int. J. Energy Res. 26 (7) (2002) 611–632.
[51] S. Lorente, E. Massias, Protection against Solar over Heatings Using High Aspect Ratio Open Vertical Cavities, World Renewable Energy Congress, Florence, 1998, pp. 20–25.
[52] R. Van Straaten, J. Straube, T. Trainor, A. Habellion, Wind Washing Effects on Mineral Wool Insulated Sheathings, 2016.
[53] C. Balocco, Transient simulation of a naturally ventilated façade in a mediterranean climate, Comsol Conf 2009 (2009) 1–5.
[54] F. Patania, A. Gagliano, F. Nocera, A. Ferlito, A. Galesi, Thermofluid-dynamic analysis of ventilated facades, Energy Build. 42 (7) (2010) 1148–1155.
[55] M. Van Belleghem, M. Steeman, A. Janssens, M. De Paepe, Heat, air and moisture transport modelling in ventilated cavity walls, J. Build. Phys. 38 (4) (2015) 317–349.
[56] A. Gagliano, F. Nocera, S. Aneli, Thermodynamic analysis of ventilated façades under different wind conditions in summer period, Energy Build. 122 (2016) 131–139.
[57] A. Gagliano, S. Aneli, Analysis of the energy performance of an Opaque Ventilated Façade under winter and summer weather conditions, Sol. Energy 205 (2020) 531–544.
[58] C. Hannan, D. Derome, A Study of Air Movement in the Cavity of a Brick Veneer Wall, 2007, pp. 1–16.
[59] C. Buratti, D. Palladino, E. Moretti, R. Di Palma, Development and optimization of a new ventilated brick wall : CFD analysis and experimental validation, Energy Build. 168 (2018) 284–297.
[60] E. Jung, Dauerstandsverhalten von Verblendziegelmauerwerk unter Witterungsbeanspurchung und Auswirkungen von Kerndämm Massnahmen. Messergebnisse aus Labor und Bauwerksuntersuchungen, Baustoffindustrie 28 (5) (1985) 185–188.
[61] K. Andersen, Ventilerede Hulrum I Vægkonstruktioner. –En Teoretisk Analyse. By Og Byg Dokumentation 001, Danish Building and Urban Research, Denmark, 2000.
[62] F. Stazi, G. Ulpiani, M. Pergolini, C. Di Perna, M. D'Orazio, The role of wall layers properties on the thermal performance of ventilated facades: experimental investigation on narrow-cavity design, Energy Build, 2020, p. 209.
[63] A. Prada, M. Baratieri, A. Gasparella, Analysis of the impact of ventilated cavities on the performance of opaque components, Build Simul Appl 2013-Janua (2013) 353–361.
[64] L.C.O. Souza, H.A. Souza, E.F. Rodrigues, Experimental and numerical analysis of a naturally ventilated double-skin façade, Energy Build. 165 (2018) 328–339.
[65] M.R. Bassett, Mc.Neil S. Drained and Vented Cavity Walls – Measured Ventilation Rates, vol. 118, 2005.
[66] M. Bassett, S. McNeil, Ventilation measured in the wall cavities of high moisture risk buildings, J. Build. Phys. 32 (4) (2009) 291–303.

[67] K. Nore, B. Blocken, J.V. Thue, On CFD simulation of wind-induced airflow in narrow ventilated facade cavities: coupled and decoupled simulations and modelling limitations, Build. Environ. 45 (8) (2010) 1834–1846.
[68] M. Labat, M. Woloszyn, G. Garnier, G. Rusaouen, J.J. Roux, Impact of direct solar irradiance on heat transfer behind an open-jointed ventilated cladding: experimental and numerical investigations, Sol. Energy 86 (9) (2012) 2549–2560.
[69] M.D. Gibson, Cool Skins : Materials and Assemblies for Ventilated Building Envelopes in Warm Climates, 2013.
[70] A. Dugué, A. Sommier, D. Bruneau, P. Lagière, Characterization and valorization of shading devices: proposition of a simple and flexible model, Plea 1 (2014) 4–11.
[71] M. González, E. Blanco, J.L. Río, J. Pistono, C. San-Juan, 447: Numerical Study on Thermal and Fluid Dynamic Behaviour of an Open-Joint Ventilated Façade, 2008.
[72] C. Mesado, S. Chiva, E. Juliá, L. Hernandez, Two dimesnional modelling with cfd of the behavior of a ventilated ceramic façade, V Eur Conf Comput Fluid Dyn ECCOMAS CFD 2010 (2010) 14–17.
[73] C. Sanjuan, M.J. Suarez, M. Gonzalez, J. Pistono, E. Blanco, Energy performance of an open-joint ventilated facade compared with a conventional sealed cavity facade, Sol. Energy 85 (2011) 1851–1863.
[74] C. Sanjuan, M. Nuria, R. Heras, E. Blanco, Experimental analysis of natural convection in open joint ventilated façades with 2D PIV, Build. Environ. 46 (11) (2011) 2314–2325.
[75] M.N. Sanchez, C. Sanjuan, M.J. Suarez, M.R. Heras, Experimental assessment of the performance of open joint ventilated facades with buoyancy-driven airflow, Sol. Energy 91 (2013) 131–144.
[76] M.N. Sánchez, E. Giancola, M.J. Suárez, E. Blanco, M.R. Heras, Experimental evaluation of the airflow behaviour in horizontal and vertical Open Joint Ventilated Facades using Stereo-PIV, Renew. Energy 109 (2017) 613–623.
[77] E. Giancola, C. Sanjuan, E. Blanco, M.R. Heras, Experimental assessment and modelling of the performance of an open joint ventilated façade during actual operating conditions in Mediterranean climate, Energy Build. 54 (2012) 363–375.
[78] M.J. Suárez, C. Sanjuan, A.J. Gutiérrez, J. Pistono, E. Blanco, Energy evaluation of an horizontal open joint ventilated faade, Appl. Therm. Eng. 37 (2012) 302–313.
[79] A. Silberstein, H. Hens, Effects of air and moisture flows on the thermal performance of insulations in ventilated roofs and walls, J. Build. Phys. 19 (1996) 367–385.
[80] A. Silberstein, E. Arquis, D.J. McCaa, Forced convection effects in fibrous insulation, in: Insulation Materials: Testing and Applications, ASTM STP1116. ASTM West, Conshohocken, PA, 1991, pp. 292–309.
[81] C. Tanner, K. Ghazi, Warmebrucken von hinterlufteten Fassaden, Duebendrof, Swtizerland, 1996. EMPA Bericht 158 740.
[82] C. Balocco, A simple model to study ventilated facades energy performance, Energy Build. 34 (5) (2002) 469–475.
[83] B. Moshfegh, M. Sandberg, Investigation of fluid flow and heat transfer in a vertical channel heated from one side by PV elements, Renew. Energy (1996) 248–253.
[84] C. Sanjuan, M. José, E. Blanco, R. Heras, Development and experimental validation of a simulation model for open joint ventilated facades, Energy Build. 43 (12) (2011) 3446–3456.
[85] F.P. Lopez, Numerical and Experimental Analysis of the Energy Saving and Potential of Ventilation of Opaque Ventilates Facades, 2012.
[86] E. SŠagát, L. Matëjka, Numerical study of the influence of insect grille on airflow in ventilated facade constructions, Adv. Mater. Res. 1041 (2014) 31–34.
[87] B. Schwarz, Witterungsbeansphruchung von Hochhausfassaden, HLH 2412 (1973) 376–384.
[88] T.D. Jacobsen, R.E. Petersen, Fugt, Varme Og Konvektion I Bygningsdele (In Danish). Master thesis at IBE, Technical University of Denmark, 1998.
[89] F. Stazi, F. Tomassoni, A. Vegliò, C.D. Perna, Experimental evaluation of ventilated walls with an external clay cladding, Renew. Energy 36 (12) (2011) 3373–3385.
[90] F. Stazi, A. Vegliò, C. Di Perna, Experimental assessment of a zinc-titanium ventilated facade in a Mediterranean climate, Energy Build. 69 (2014) 525–534.